

UNIVERSITY OF JORDAN
FACULTY OF GRADUATE STUDIES


**HEAT TRANSFER IN EXTERNAL STONE WALLS:
THE EFFECT OF STONE SURFACE TEXTURE**

By

YOUSEF MOH'D-SAID IBRAHIM

Supervised by

Dr. ALI BADRAN

عميد كلية الدراسات العليا


Submitted in partial fulfillment of the requirements for the degree of

Master of Science in
Mechanical Engineering
Faculty of Graduate Studies
University of Jordan

December, 1995

٢٠١٥

This theses was defended successfully on 25/12/1995

COMMITTEE MEMBERS

SIGNATURE

Dr. Ali Badran

A. Badran

Prof. Mohammed Hamdan

[Signature]

Prof. Bassam Jubran

B. Jubran

DEDICATION

TO THE MEMORY OF MY FATHER

MY MOTHER

BROTHERS AND SISTERS

ACKNOWLEDGEMENT

I would like to convey my sincere gratitude to my supervisor *Dr. Ali Badran* for his close supervision, indispensable encouragement, valuable discussions and guidance throughout all stages of this work.

Great thanks are also extended to *Prof. Mohammed Hamdan* and *Prof. Bassam Jubran* for their suggestions and fruitful discussions.

My thanks are sent out to all my friends and colleagues who supported me during this work, and appreciation and special thanks to my brothers and sisters especially my brother *Bilal* who helped me in the experimental part of this work.

Finally, special gratitude is regarded to my mother for her constant support and encouragement.

TABLE OF CONTENTS

COMMITTEE DECISION	II
DEDICATION	III
ACKNOWLEDGMENT	IV
TABLE OF CONTENTS	V
LIST OF TABLES	VIII
LIST OF FIGURES	X
NOMENCLATURE	XII
ABSTRACT	XIV
<u>CHAPTER 1: INTRODUCTION</u>	1
1.1 Significance of This Work	3
<u>CHAPTER 2: LITERATURE SURVEY</u>	6
<u>CHAPTER 3: THEORETICAL ANALYSIS</u>	21
3.1 Data Reduction	21
3.2 Theoretical Analysis	23
3.2.1 Convective Heat-Transfer Coefficient	23
3.2.2 Fin Model	24

3.2.3	Fin Effectiveness	29
3.2.4	Array of Fins	31
3.2.5	Estimation of Fin Dimensions	34
3.2.6	Fin Heat Transfer Rate	40
<u>CHAPTER 4: EXPERIMENTAL RIG AND PROCEDURE</u>		42
4.1	Introduction	42
4.2	The Apparatus	44
4.3	The Metering Box	49
4.4	The Guard Box	50
4.5	The Cold Box	51
4.6	The Sample Frame	54
4.7	Measuring Devices	55
4.7.1	Temperature Measurement	55
4.7.2	Heat Input Measurement	56
4.7.3	Air Velocity Measurement	57
4.8	Experimental Work Procedure	57
<u>CHAPTER 5: DATA AND CALCULATIONS</u>		62
5.1	Experimental Results	62
5.2	Error Analysis	71

	VII
5.3 Fin Model Results	76
<u>CHAPTER 6: DISCUSSION</u>	83
6.1 Introduction	83
6.2 Effect of Surface Texture	83
6.3 Effect of Wind Speed	86
6.4 Theoretical Fin Model Compared with Experimental Results	88
<u>CHAPTER 7: CONCLUSIONS & RECOMMENDATIONS</u>	94
7.1 Conclusions	94
7.2 Recommendations	96
<u>REFERENCES</u>	98
<u>APPENDIX A: DATA TABLES</u>	102
<u>APPENDIX B: SAMPLE CALCULATIONS</u>	126
<u>ABSTRACT (IN ARABIC)</u>	128

LIST OF TABLES

Table 5.1	Results for smooth-surface wall ($v = 1.6$ m/s)	63
Table 5.2	Results for smooth-surface wall ($v = 0.5$ m/s)	64
Table 5.3	Results for hammered wall ($v = 1.6$ m/s)	65
Table 5.4	Results for hammered wall ($v = 0.5$ m/s)	66
Table 5.5	Results for punched wall ($v = 1.6$ m/s)	67
Table 5.6	Results for punched wall ($v = 0.5$ m/s)	68
Table 5.7	Results for rough-surface wall ($v = 1.6$ m/s)	69
Table 5.8	Results for rough-surface wall ($v = 0.5$ m/s)	70
Table 5.9	Uncertainties in the basic measurements (Q, l and T)	71
Table 5.10	Uncertainties in the measurements of U, K and h ($v = 0.5$ m/s)	75
Table 5.11	Uncertainties in the measurements of U, K and h ($v = 1.6$ m/s)	75
Table 5.12	Estimation of number of fins and volumes of the walls	77
Table 5.13	Fin dimension for rectangular fin model	77
Table 5.14	Fin dimension for pin fin model	78
Table 5.15	Fin dimension for trapezoidal fin model	78
Table 5.16	Theoretically evaluated (model) heat transfer rate	81
Table 5.17	Theoretically evaluated (model) convective heat-transfer coefficients	82
Table 5.18	Theoretically evaluated (model) overall heat-transfer coefficients	83

Table 6.1	The relation between the type of the wall and heat-transfer coefficients	84
Table 6.2	The relation between the wind speed and heat transfer	86
Table 6.3	Theoretical values of h (all walls)	87
Table 6.4	Length of fins	91
Table 6.5	Convective heat transfer coefficient (model versus experiment)	92
Table 6.6	Overall heat transfer coefficient (model versus experiment)	93

LIST OF FIGURES

Fig. 1.1:	Pictures of the four different stones	5
Fig. 2.1:	Schematic of test geometry: (a) ribbed; (b) stepped	11
Fig. 2.2:	Composite interferogram of a typical ribbed test section	12
Fig. 2.3:	Composite interferogram of typical stepped test section	12
Fig. 2.4:	Local heat transfer coefficient for ribbed plate with $p/s=8:1$ and $p/q=8:1$	13
Fig. 2.5:	Schematic of sinusoidal test section [12]	15
Fig. 2.6:	Photograph of the sinusoidal test section with amplitude-to-wavelength ratio = 0.3 [12]	15
Fig. 2.7:	Composite interferogram of sinusoid test section with amplitude-to-wavelength ratio = 0.1 [12]	16
Fig. 2.8:	Local heat transfer coefficient for sinusoidal plate with amplitude-to-wavelength ratio = 0.05 [12]	17
Fig. 2.9:	Local heat transfer coefficient for sinusoidal plate with amplitude-to-wavelength ratio = 0.1 [12]	17
Fig. 2.10:	Local heat transfer coefficient for sinusoidal plate with amplitude-to-wavelength ratio = 0.3 [12]	18
Fig. 3.1:	Examples of extended surfaces: (a) rectangular; (b) pin fin and (c) trapezoidal fin	27
Fig. 3.2:	Array of rectangular fins	31
Fig. 3.3:	Sand box	36
Fig. 3.4:	Picture of the sand box	36
Fig. 4.1:	Purpose of the test	43

Fig. 4.2:	General arrangements of the test box, guard box, test panel and cold box	46
Fig. 4.3:	Schematic diagram of the apparatus used in the experiment	47
Fig. 4.4:	A photograph of the guarded hot box apparatus	48
Fig. 4.5:	A photograph of the metering box	48
Fig. 4.6:	A photograph of the cold box	53
Fig. 4.7:	A photograph of the sample frame	54
Fig. 4.8:	A photograph showing the instruments of temperature and heat input read outs	55
Fig. 4.9:	Building up the wall inside the frame	58
Fig. 4.10:	A photograph showing the thermocouples fixed on the wall	59
Fig. 5.1	Temperature distribution through smooth wall ($v=1.6$ m/s)	63
Fig. 5.2	Temperature distribution through smooth wall ($v=0.5$ m/s)	64
Fig. 5.3	Temperature distribution through hammered wall ($v=1.6$ m/s)	65
Fig. 5.4	Temperature distribution through hammered wall ($v=0.5$ m/s)	66
Fig. 5.5	Temperature distribution through punched wall ($v=1.6$ m/s)	67
Fig. 5.6	Temperature distribution through punched wall ($v=0.5$ m/s)	68
Fig. 5.7	Temperature distribution through rough wall ($v=1.6$ m/s)	69
Fig. 5.8	Temperature distribution through rough wall ($v=0.5$ m/s)	70

NOMENCLATURE

- A_f : Exposed surface area of fins only (m).
 A_p : Cross-sectional area of the pin fin (m^2).
 A_r : Cross-sectional area of the rectangular fin (m^2).
 A_s : Area of a single stone (m^2).
 A_t : Cross-sectional area of the trapezoidal fin (m^2).
 A_{tot} : Total exposed surface area including the fins and unfinned surface.
 A_w : Area of the wall (m).
 D : Diameter of pin fins (m).
 h : Convective heat transfer coefficient of air in the cold room ($W/m^2 \cdot ^\circ C$).
 h_{th} : Theoretical heat-transfer coefficient ($W/m^2 \cdot ^\circ C$).
 k : Conductivity of the stone ($W/m^2 \cdot ^\circ C$).
 l : Thickness of the wall (m).
 L : Length of the fin (m).
 Q : Heat transfer rate (W).
 T_c : Temperature of the cold room ($^\circ C$).
 T_h : Temperature of the cold hot ($^\circ C$).
 T_1 : Temperature of the of wall hot surface ($^\circ C$).
 T_2 : Temperature of the of wall cold surface ($^\circ C$).

- U : Overall heat-transfer coefficient ($\text{W}/\text{m}^2 \cdot ^\circ\text{C}$).
- v : Wind speed (m/s).
- V_f : Volume of the array of fins (m^3).
- V_t : Total volume of fins and voids (m^3).
- V_v : Void volume between the fins (m^3).
- w_r : Width of the rectangular fin (m).
- w_t : Width of the trapezoidal fin (m).
- δ : Spacing between the centers of the fins (m).
- ϕ : Fin effectiveness.
- η : Total surface temperature effectiveness.

ABSTRACT

“Heat Transfer in External Stone Walls: The Effect of Stone Surface Texture”

By

Yousef Moh'd-Said Ibrahim

Supervised by

Dr. Ali Badran

In this work, the effect of surface texture of stone walls on heat transfer was investigated. Special emphasis were placed on this effect on the overall heat - transfer coefficient of the wall. The investigation was carried out experimentally and theoretically. The experimental work was carried out using the ASTM standard test method designated by C-236. The guarded hot box apparatus was used to test thermally four different stone walls common in Jordan, and the stone walls used in the experiment were of the types of the saw-cut-surface, the hammered or the locally called

“Musamsam”, the punched “Mufajjar” and the rough-surface “Tobzeh” walls.

It was experimentally found that, among the four walls tested under the same heat input, the overall heat transfer coefficient of the rough-surface “Tobzeh” stone wall has the largest U factor. Then next in heat transfer coefficient was the punched “Mufajjar”, then the hammered “Musamsam” and finally the saw-cut stone wall.

Theoretical investigation was carried out to find a mathematical model for heat transfer in these types of stone walls. The model investigated was that of a plane wall with fins which represent the roughness existent in the stone surface texture. The fin models under investigation were the rectangular, pin and trapezoidal fin models. The models show that they produce close results as those of the experimental data, especially the trapezoidal fin model which gives a good simulation of the rough-surface wall.

CHAPTER 1

INTRODUCTION

The subject of heat transfer has a great impact on all energy problems, covering the range from the routine task of heating or cooling buildings to the problems associated with nuclear power generation. As energy costs have increased, there has been an increasing awareness of the impact on energy consumption in structures. The tools of prediction and evaluation of building energy consumption may differ in complexity and form, but they must account for the three heat transfer processes (radiation, conduction, and convection) that take place within the building and between the building and the environment. While radiation and conduction in the temperature range applicable to buildings are well understood, convection heat-transfer processes which have the highest contribution in the building thermal performance calculations among the other heat transfer modes are typically dealt with in an imprecise way. The understanding of the influence of convective heat-transfer processes on the thermal performance of buildings is necessary to enable the designer and the analyst to i) predict the influence of design decisions on the energy consumption of a building and/or ii)

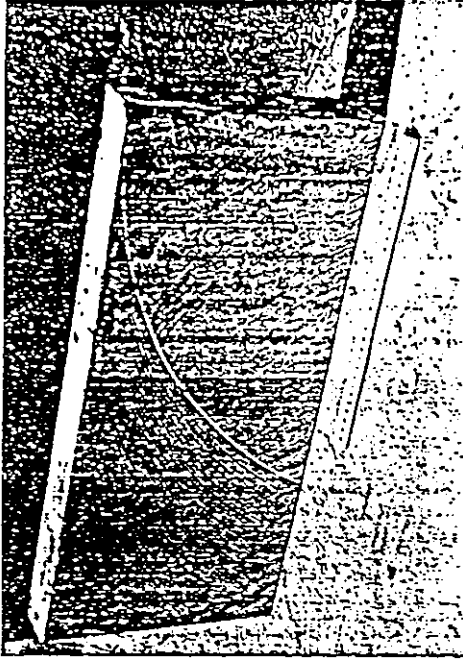
interpret the performance of the building in order to obtain a basis for design decision in future projects.

Most of the previous studies and analysis of heat-transfer through building materials did not take into consideration the texture of stone walls. It is known that in many countries the buildings are constructed mainly from stone walls with different textures. Thus it becomes important to study the texture of stone walls in terms of heat transfer especially the branch of convection heat transfer.

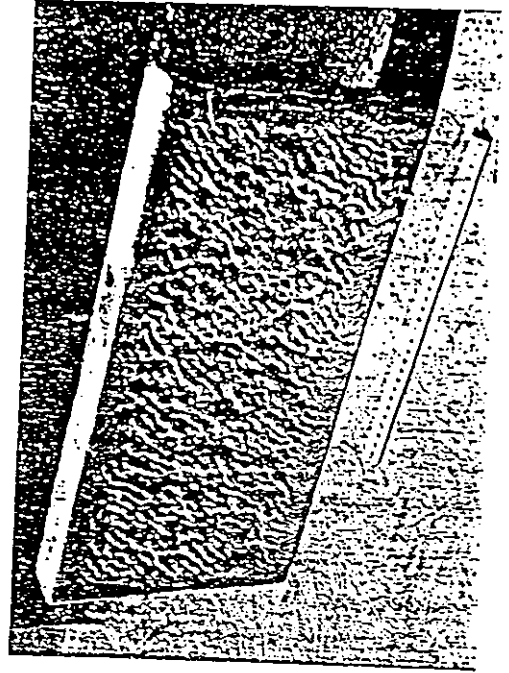
Since the experimental work of Ray in 1920 [1], heat convection has developed into one of the most studied topics in heat transfer. However, relatively little theoretical information is available of the effect of complex geometries on convection heat transfer. Several studies have examined the effect of roughness on average heat transfer coefficients for vertical surfaces. In addition, the accurate values of heat transfer are very important and vital for many applications. In building design, in order for energy to have an appropriate weight in decisions, accuracy in energy calculations must be provided.

increases the surface area of the wall; Thereby the heat transfer is increased in a fashion similar to that caused by extended surfaces and fins.

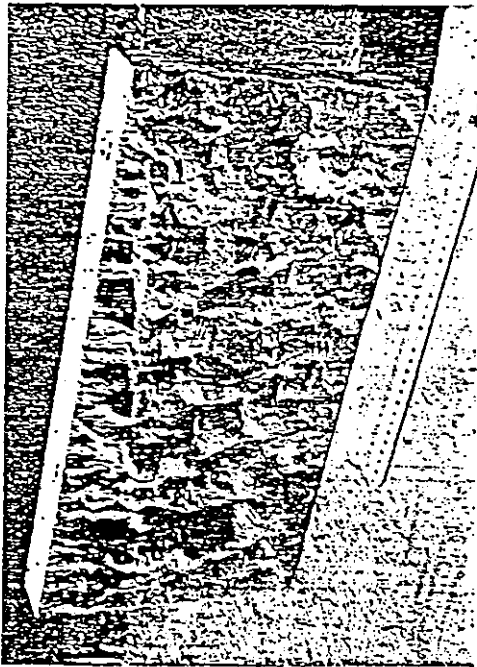
The purpose of this research is to find values of the overall heat transfer coefficient for various types of local external stone walls experimentally. Four types of local stone walls is investigated: Saw-cut-type (smooth surface), Hammered “Musamsam”, Punched “Mufajjar” and Rough surface type “Tubzeh” (Fig. 1.1).



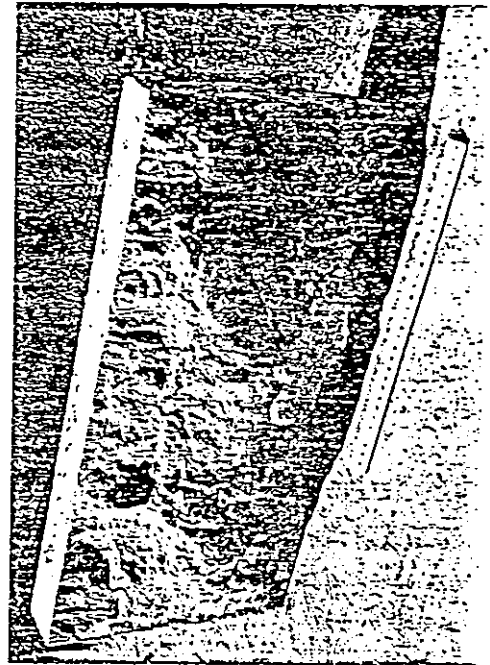
(a)



(b)



(c)



(d)

Fig. 1.1: Pictures of the four different stones: (a) Saw-cut, (b) Hammered “Musamsam”, (c) Punched “Mufajjar” and (d) Rough-surface “Tobzeh” stones.

CHAPTER 2

LITERATURE SURVEY

An understanding of heat transfer is essential for proper design of building systems, particularly for those buildings where passive cooling and heating techniques are employed. Most of the past experimental and analytical work on convection heat transfer from surfaces have focused on smooth surfaces. However, the surfaces of buildings are seldom smooth. The inclusion of surface roughness on heat convection study is of interest from a fundamental point of view because the effect of roughness on heat convection flows are not very well understood. It should be clear, however, that no previous work was found on rough building surfaces of the types available in local stones. This type of roughness is characterized by being highly irregular and of sizes that are beyond the scope of previous works. Therefore, this survey is intended to show the frontiers of the previous works rather than to show a connection with those works because, in fact, there is no real connection.

The earliest experiments on the effects of surface roughness on heat transfer are carried out by Prasolov [4] using distributed roughness elements on the outside surface of horizontal cylinder. The experiments were carried out in air in the laminar - to - turbulent transition regime. roughness heights varied from 0.08 to 0.36 mm. Prasolov attributed the increase in heat transfer to “turbulization” of the flow in the transitional regime. He also found that the effect of surface roughness on heat transfer depends on the temperature difference between the wall and the adjacent fluid and the type of the fluid itself.

Jofre and Barron [5] made their experiments with an isothermal vertical plate in air. The rough surface consisted of horizontal ribs with triangular cross sections which were 0.76 mm high. Based upon comparisons with smooth plate experiments by Eckert and Jackson [6] they found that the rough surface increased the heat transfer by a factor of about two.

Fujii, Fujii and Takeuchi [7] examined the effect of rough surfaces on heat transfer from a vertical cylinder with a constant surface heat flux. They studied the case with water and oil using a variety of rough surfaces and

found the maximum difference in the local heat transfer in the turbulent regime to be of the order of 10 percent.

Sastry, Murthy and Sarma [8] examined the effect of roughness created by wrapping various gauges of copper wire around a vertical cylinder. They found that the overall heat transfer was enhanced by up to 50 percent over that of a smooth cylinder. They were apparently unaware of the earlier work of Fujii et al., and thus did not attempt to explain the difference between their results and the previous ones.

Anderson and Bohn [9] identified two distinctly different ways by which the natural convection heat transfer coefficient may be altered due to roughness. The roughness may introduce disturbances into an overlying laminar boundary layer, which causes the boundary layer to be in the turbulent regime. Thus the part of the wall that is exposed to turbulent flow, which in absence of the roughness would have been in laminar flow, experiences heat transfer augmentation. Another way in which heat transfer may be altered is through various mechanisms associated with the locally altered flow near the roughness element. The heat transfer in fully separated zones may be reduced compared to that of the same location on a smooth surface. They made their experimental study on the effect of one type of

surface roughness upon heat transfer in a water - filled cubical enclosure. The roughness elements used in the experiment consisted of a series of intersecting grooves. The height of the elements was chosen to be the same order of magnitude as the thickness of the thermal boundary layer evaluated analytically. It was concluded that for an isothermal surface, the rough texture reduced the location of transition by about 5 percent. The results of their study confirm that the surface roughness can be used to produce heat transfer enhancement in enclosure flows. They concluded that there is a need for further researches with other types of roughness elements to determine if the large increase in local heat transfer which were measured in their experiment can be extended to produce a larger effect upon the overall heat transfer.

455763

In another recent study, Shakerin et al. [10] determined the heat transfer characteristics in an enclosure with square-cross-sectioned ribs on the heated wall. The height of their roughness elements was a multiple of the boundary layer thickness at the centre of the smooth walled enclosure. The study was conducted experimentally using a Mach-Zehnder interferometer and was supported by numerical calculations. The enhancement obtained with two ribs suggested that the spacing of roughness elements may be important.

Bhavnani and Bergles [11] made their experimental studies using interferometric technique to determine local heat transfer coefficients for surfaces with repeated ribs and steps (Fig. 2.1). They found that heat transfer enhancement was possible in laminar natural convection using transverse roughness elements of proper size and shape. The maximum increase in average heat transfer coefficient was 32 percent with a step pitch-to-height ratio of 16.

Composite interferograms of typical ribbed and stepped test sections are shown in Figs. 2.2 and 2.3. Fig. 2.4 shows the variation of local heat transfer coefficients for a ribbed test section with rib-to-height ratio of 8:1 and pitch-to-width ratio of 8:1.

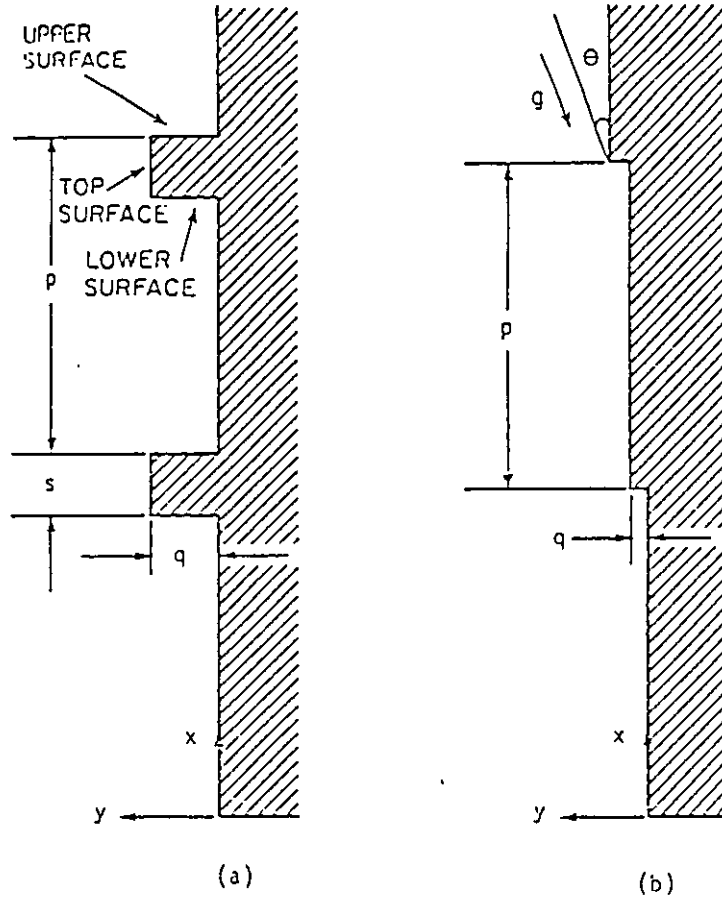


Fig. 2.1: Schematic of test geometry: (a) ribbed; (b) stepped



Fig. 2.2 Composite interferogram
of a typical ribbed test
section

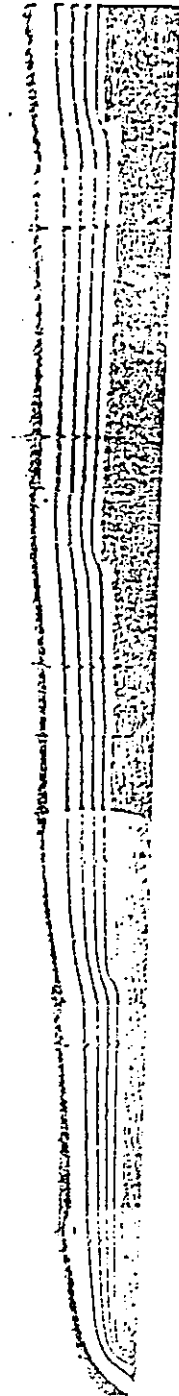


Fig. 2.3 Composite interferogram
of a typical stepped test
section

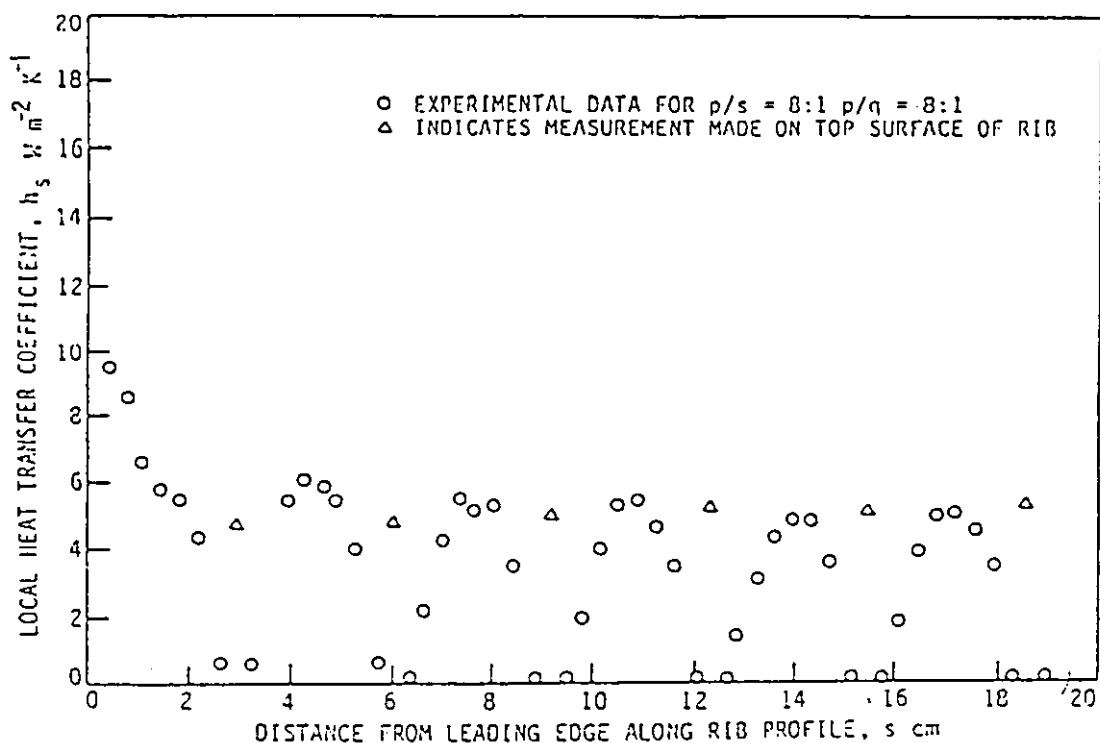


Fig. 2.4: Local heat transfer coefficient for ribbed plate with $p/s=8:1$ and $p/q=8:1$

Another method of study was done by Bhavnani and Bergles [12]. They studied experimentally the heat transfer characteristics of sinusoidal wavy surfaces on vertical plates maintained at a constant temperature. A Mach-Zehnder interferometer (MZI) was used in this experimental study. A schematic of the test is shown in Fig. 2.5. Test sections were fabricated from aluminium plate. The length of the test section was 152.4 mm. Three test sections with amplitudes 2.54 mm, 5.08 mm and 15.24 mm were used which represent a roughness of high order. The lengths of the amplitudes resulted

in amplitude-to-wavelength ratios of 0.05, 0.1 and 0.3, respectively. A photograph of a single test section is shown in Fig. 2.6. a composite interferogram of the test section with amplitude-to-wavelength 0.1 is shown in Fig. 2.7. Figures 2.8 to 2.10 show the data obtained with the sinusoidal surfaces mentioned above. The heat transfer performance was evaluated by comparing the experimental data with the analytical one. The heat transfer using the surface with amplitude-to-wavelength of 0.05 was 1.6% greater than that for a plane plate of equal projected area. The increase in heat transferred was up to 5.0% for the surface with amplitude-to-wavelength of 0.1 and to 14.1% for the surface with amplitude-to-wavelength of 0.3. The conclusion of their experimental study was that the heat transfer from the wavy surfaces, compared to a plane plate of equal projected area, was enhanced with increasing amplitude-to-wavelength ratios. Furthermore, they found that increasing the amplitude-to-wavelength ratio of the sinusoidal surface resulted in an unstable thermal boundary layer which confirms that rough surfaces induce an early transition to turbulence due to the destabilizing effects of the transverse velocity component.

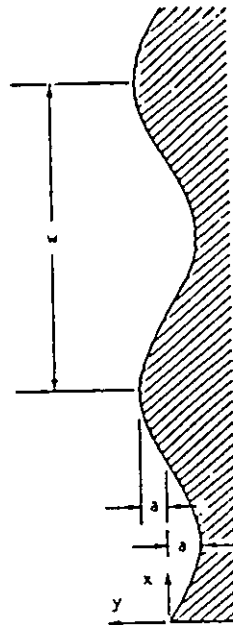


Fig. 2.5: Schematic of sinusoidal test section [12]

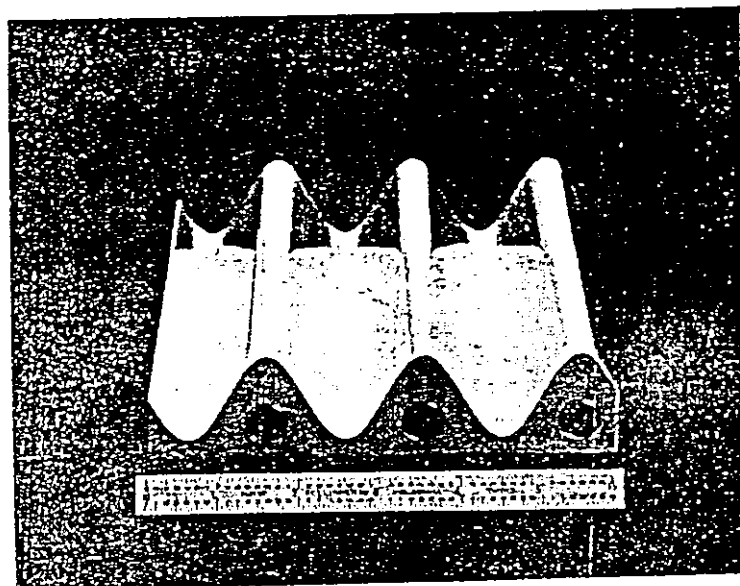


Fig. 2.6: Photograph of the sinusoidal test section with amplitude-to-wavelength ratio = 0.3 [12]

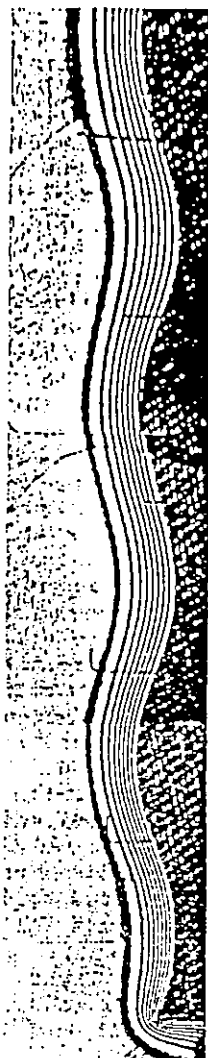


Fig. 2.7: Composite interferogram of sinusoidal test section with amplitude-to-wavelength ratio = 0.1[12]

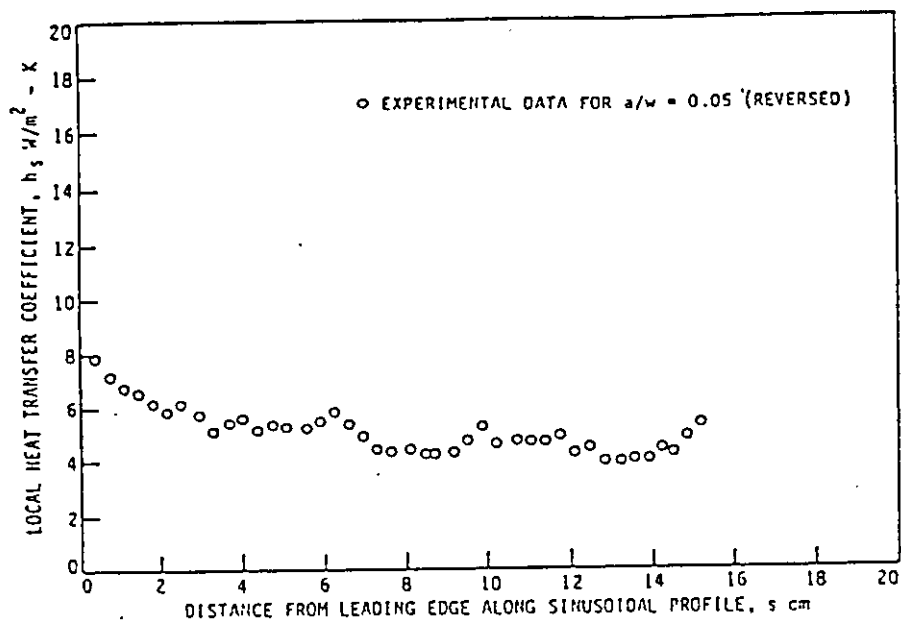


Fig. 2.8: Local heat transfer coefficient for sinusoidal plate with amplitude-to-wavelength ratio = 0.05 [12]

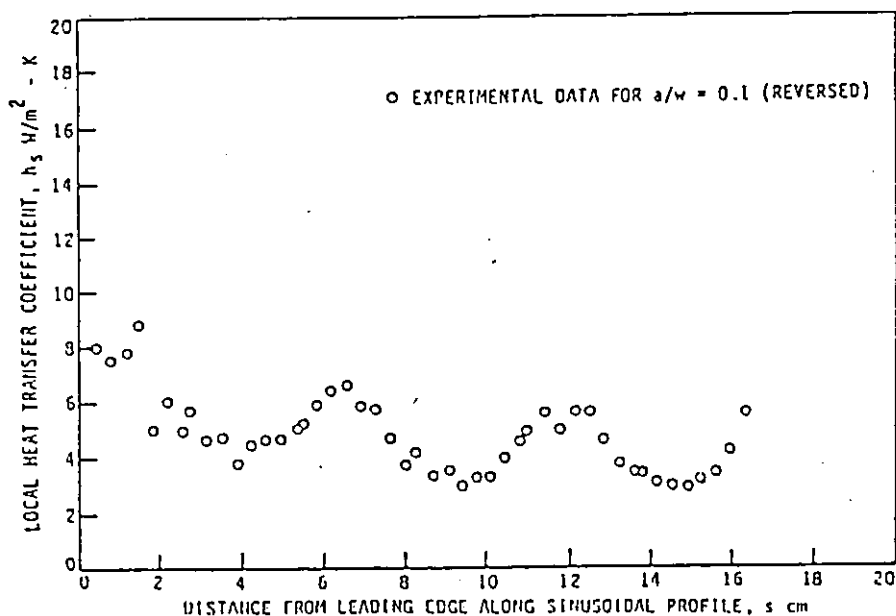


Fig. 2.9: Local heat transfer coefficient for sinusoidal plate with amplitude-to-wavelength ratio = 0.1 [12]

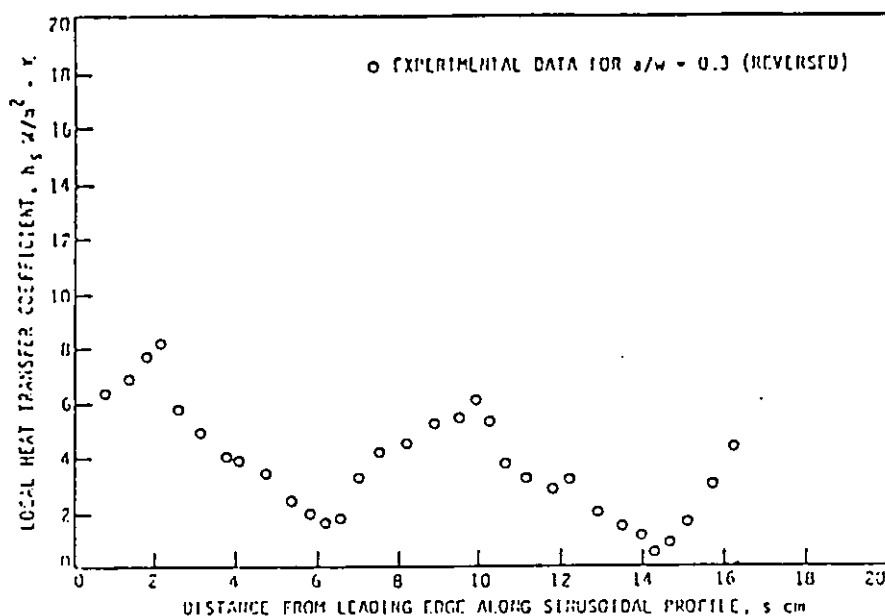


Fig. 2.10: Local heat transfer coefficient for sinusoidal plate with amplitude-to-wavelength ratio = 0.30 [12]

Another study of the thermal performance of wavy surfaces, which are representations of surfaces of high order of roughness, was done by Kishinami et. al. [13]. In their study, convection heat transfer from a vertical wavy surface has been investigated experimentally for the combination of isothermally heated concave and unheated convex semicircular elements, and the opposite heating combination. A Mach-Zehnder interferometer was used. They concluded that the average Nusselt number has a tendency to decrease up to the third wave of the surface, to increase slightly to the fourth and fifth waves and to decrease after that.

Hosni et. al.[14] conducted their study on rough-wall heat transfer in the turbulent boundary layer. They used four different surfaces in their experiments. Their work was concerned with heat transfer in smooth, transitionally rough, and fully rough flow regimes. They conducted their experiments for the incompressible flow of air over three rough surfaces for a range of free stream velocity which gives Reynold's numbers up to 1×10^7 . The three rough surfaces were composed of 1.27 mm diameter hemispherical elements spaced 2, 4 and 10 diameters apart, respectively, in staggered arrays on otherwise smooth walls. As a result of their experimental investigation, Stanton number (which is an indication of heat transfer in forced convection) are now available over a wide range of Reynold's number for the three well-defined rough surfaces. The results of the three rough surfaces indicate that there is a different relation between Stanton number and Reynold number for each surface. Furthermore, the Stanton number at a given Reynold number increases with decreasing roughness spacing, that is, as the surface becomes 'rougher'. The results indicate also that the magnitude of the roughness effect on heat transfer increases with decreased roughness element spacing only up to some 'roughest' spacing, and as roughness element spacing is decreased more (and approaches the most densely packed configuration), the magnitude of the roughness effect on heat transfer diminishes.

In summary, most of the past researches in convection heat transfer has been oriented toward metallic surface applications rather than heat-transfer in stone building materials [15], while the convection problem as it relates to building external walls clearly has not been addressed .

CHAPTER 3

THEORETICAL ANALYSIS

In this chapter, the equations used in the calculation and modeling are discussed, and the mathematical model for the walls is deduced.

3.1 Data Reduction

In calculating heat transfer through walls one may use the following equation which gives the overall heat-transfer coefficient (U) provided that the amount of heat transfer (Q) is known and the temperatures of both sides of wall are known:

$$U = \frac{Q}{A(T_h - T_c)} \quad (3.1)$$

And if the temperatures at the wall surfaces T_1 and T_2 are known, the thermal conductivity of the wall material may be calculated from the equation:

$$k = \frac{Q \times l}{A(T_1 - T_2)} \quad (3.2)$$

Similar equations may be used to calculate the inside and the outside heat-transfer coefficients h_i and h respectively:

$$h_i = \frac{Q}{A(T_h - T_1)} \quad (3.3,a)$$

$$h = \frac{Q}{A(T_2 - T_c)} \quad (3.3,b)$$

The above four equations yield the overall heat-transfer coefficient of the wall, the conductivity of the wall and the convection heat-transfer coefficient of the air at the cold and the hot sides of the wall, respectively. With the exception of h , all the parameters in the previous equations are usually taken as constants properties. For example, h_i is constant because all the walls are usually smooth at the inside and still air conditions exist there, which means all the parameters that affect the value of the convective heat transfer coefficient in the hot side is kept constant for all walls. The basic variable is h which depends on the texture of the external wall surface and the wind speed.

3.2 Theoretical Analysis:

3.2.1 Convective Heat-transfer Coefficient

The convective heat-transfer coefficient expressed in equation (3.3) may be expressed theoretically by the correlation adopted by ASHRAE [2] in which h is given by:

$$h_{th} = 5.62 + 3.9 v \quad (3.4)$$

Equation (3.4) is applicable for the following conditions:

- The surface is a vertical plane.
- The fluid is air.
- The velocity of the air (v) is less than 5 m/s.
- Forced convection.
- The temperature of the fluid is between 0°C and 25°C

There are other equations for vertical plane surfaces which are velocity dependent but are for velocities greater than 5 m/s. Based on equation (3.4) the theoretical convective heat-transfer coefficient may now be computed.

When calculating the theoretical values of the convective heat-transfer coefficient for a wall of a certain texture, it is assumed that these values depend only on the wind speed and, because of the capability of the apparatus used in the experiment, one is 0.5 m/s and the other is 1.6 m/s.

Using equation (3.4) one may have only two values of the theoretical convective heat-transfer coefficient for all cases. One for air speed of 0.5 m/s where $h_{th} = 7.57 \text{ W/m}^2\cdot\text{K}$ and the other for air speed of 1.6 m/s where $h_{th} = 11.86 \text{ W/m}^2\cdot\text{°C}$. In this case it is easy to tabulate these results since there are only two values of h_{th} .

3.2.2 Fin Model

The difference between the smooth-surface wall and the other wall types is that the other types can be divided into two parts, one is the basic surface wall, and the other is the extra irregular - shape or roughness which basically increases the surface area. The irregular part of the wall may be modelled to act like a finned surface. Since the stone has an irregular texture, it is difficult to model the wall with a specific type of fins. There are different types of fins, the most common of which is the longitudinal. The longitudinal fin can be with rectangular, trapezoidal or an arbitrary cross section and it acts like ribs attached along the length of a surface as shown in Fig. 3.1. The equation that represents this type of fins is as follows [16]:

$$Q_r = kmA_r(T - T_c) \frac{\sinh(mL) + (h / mk) \cosh(mL)}{\cosh(mL) + (h / mk) \sinh(mL)} \quad (3.5)$$

From equations (3.5) and (3.6) it is recognized that the only parameters that are unknown (i.e. not included in the experimental equations) are L, A and P, and from equations (3.7) to (3.10), P and A are related to each other and these equations can be rewritten as:

for a rectangular fin of unit depth:

$$A_r = \frac{1}{2} P_r - 1 \quad (3.11)$$

and for a pin fin:

$$A_p = \frac{P_p D}{4} \quad (3.12)$$

The parameter L represents the length of the fin, (i.e. the amount the fin is protruding the surface) and since the wall has an irregular texture, then the parameter (L) represents the average height of the irregularities of the stone surface.

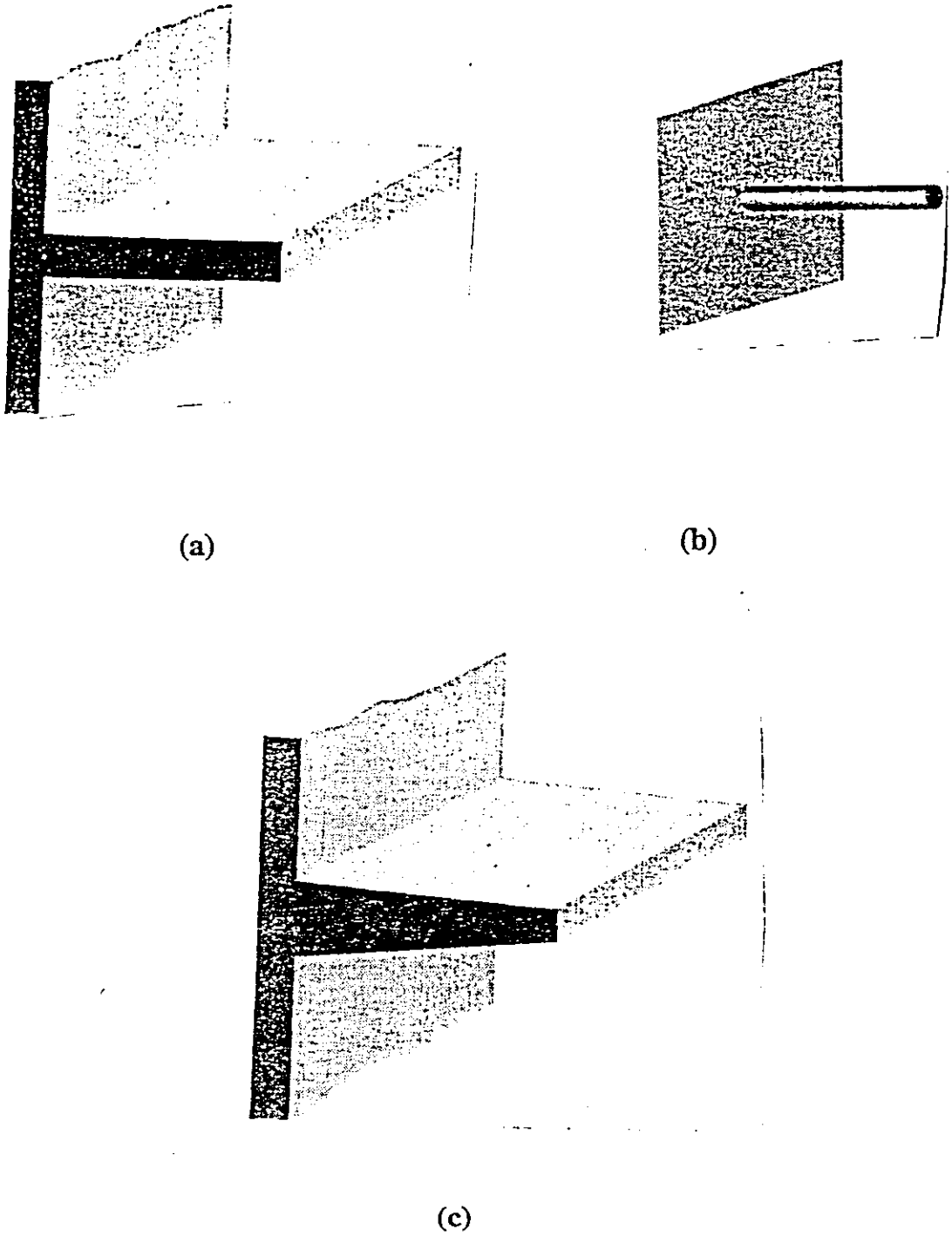


Fig. 3.1: examples of extended surfaces: (a) rectangular fin, (b) pin fin and (c) trapezoidal fin

Equations (3.5) to (3.12) are applicable for pin fins and longitudinal fin of rectangular (uniform) cross-section (Fig. 3.1,a and b). Another type of fins is the longitudinal fin of a trapezoidal (non uniform) cross - sectional area (Fig. 3.1,c). It is complicated to derive the equation of the trapezoidal fin since it has a non - uniform cross - sectional area. An analytical study was done by Chapman [17] on the trapezoidal fins, and an expression for the heat flow was concluded as follows :

$$Q_t = \frac{kw_t R}{\sqrt{L_t}} (T - T_c) \frac{I_1(2RL_t^{1/2})}{I_0(2RL_t^{1/2})} \quad (3.13)$$

Where:

$$R = \sqrt{\frac{2fhL_t}{kw_t}} \quad (3.14)$$

and

$$f = \sqrt{1 + \left(\frac{w_t}{2L_t}\right)^2} \quad (3.15)$$

L_t is the length of the trapezoidal fin. w_t is the width of the trapezoidal fin.

I_0 is the modified Bessel's function of the first kind and of order 0, and I_1 is the modified Bessel's function of the first kind and of order 1.

3.2.3 Fin Effectiveness:

Following the analysis of Chapman [17] the fin effectiveness may be analysed as follows:

The term fin effectiveness is defined as “the ratio of the heat transfer rate from a fin to the heat transfer rate that would be obtained if the entire fin surface area were to be maintained at the same as the primary surface” [17]. The relations mentioned earlier for the heat flow from various fin shapes may now be used to deduce equations for the fin effectiveness.

The relations to be developed in this section will simply present the fin effectiveness as functions of the pertinent thermal and geometric parameters.

The Straight Fin of Uniform Thickness (Rectangular Fin):

The surface area of the fin per unit depth is $2L$ so the fin effectiveness (Φ_r) is given as

$$\Phi_r = \frac{Q_r}{2L_r h \Delta T} \quad (3.16)$$

and from equation (3.5) then equation (3.16) can be rewritten as:

$$\Phi_r = \frac{1}{mL_r} \tanh(mL_r) \quad (3.17)$$

The Straight Fin of Trapezoidal Profile:

If the same procedure is followed, equation (3.13) leads to the following expression for the fin effectiveness (Φ_t) for a trapezoidal fin

$$\Phi_t = \frac{f}{L_t^{1/2} R} \frac{I_1(2RL_t^{1/2})}{I_0(2RL_t^{1/2})} \quad (3.18)$$

Pin Fin

The effectiveness of the pin fin can be calculated using the same procedure:

$$\Phi_p = \frac{1}{mL_p} \tanh(mL_p) \quad (3.19)$$

3.2.4 Array of Fins [17]

The theory discussed in the foregoing section is concerned with describing the performance of a single fin. However, many applications (like the case of this work) employing extended surfaces involve the use of an array of fins attached to the primary surface. Fig. 3.2 depicts such arrays for straight fins. In such applications it is useful to define a total surface temperature effectiveness which gives a measure of the performance of the total exposed surface of the array of fins, that is, both the finned and unfinned surface.

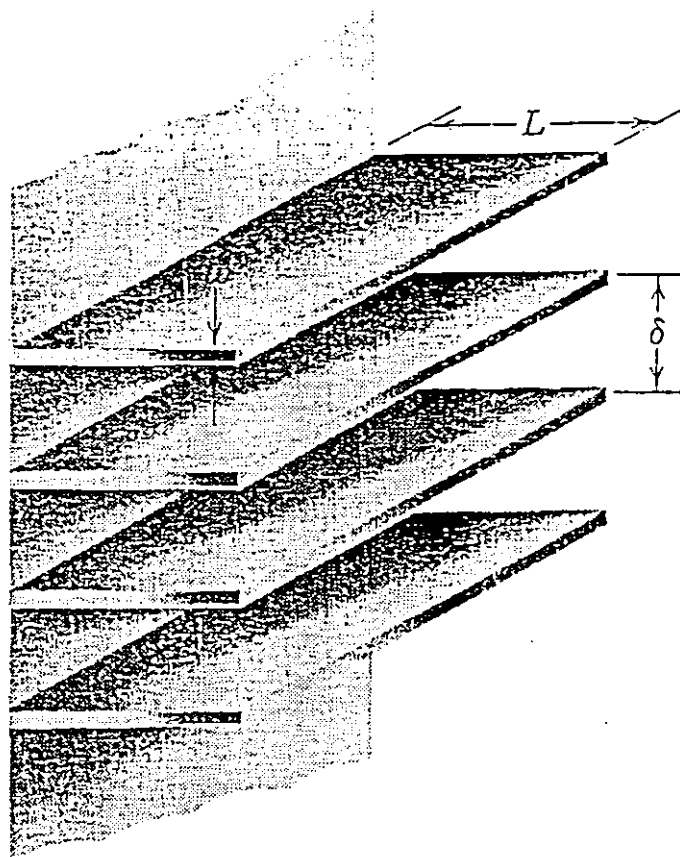


Fig. 3.2: Array of rectangular fins

Let

A_f = exposed surface area of fins only.

A_{tot} = Total exposed surface area, including the fins and unfinned surface.

Φ = effectiveness for a particular fin shape involved.

Then if the total surface temperature effectiveness (η) is defined as “the ratio of the actual heat transfer by the array to that it would transfer if its entire surface were maintained at the base temperature”,

$$\eta = \frac{(A_{tot} - A_f)h\Delta T - A_f h\Delta T\Phi}{A_{tot}h\Delta T} \quad (3.20)$$

Or

$$\eta = 1 - \frac{A_f}{A_{tot}}(1 - \Phi) \quad (3.21)$$

Since $A_f/A_{tot} < 1$ and $\Phi \leq 1$, it is apparent that $\eta \leq 1$. The values of A_f and A_{tot} (or the ratio A_f/A_{tot}) is readily evaluated from geometry of the array. For example, for an array of a uniform (rectangular) fins of length L , thickness w , spacing on centers δ and number of fins n (as shown in Fig. 3.2), one may deduce

$$A_f = n(2L + w) \quad (3.22)$$

$$A_{tot} = n(2L + w) + n(\delta - w) \quad (3.23)$$

$$A_{tot} = n(2L + \delta) \quad (3.24)$$

this implies that

$$\left(\frac{A_f}{A_{tot}} \right) = \frac{2L + w}{2L + \delta} \quad (3.25)$$

Similarly for a trapezoidal fin

$$A_f = (2L + w_2) \times n \quad (3.26)$$

$$A_{tot} = n(2L + w_2) + n(\delta - w_1) \quad (3.27)$$

$$A_{tot} = n[2L + \delta - (w_1 - w_2)] \quad (3.28)$$

$$\left(\frac{A_f}{A_{tot}} \right)_t = \frac{2L + w_2}{2L + \delta - (w_1 - w_2)} \quad (3.29)$$

For an array of pin fins:

$$A_f = n \left(\pi DL + \frac{\pi D^2}{4} \right) \quad (3.30)$$

$$A_{tot} = n \left(\pi DL + \frac{\pi D^2}{4} \right) + A_w - n \frac{\pi D^2}{4} \quad (3.31)$$

$$A_{tot} = n\pi DL + A_w \quad (3.32)$$

If heat is to be transferred through a plane wall in which the left side is the hot side where the air is at temperature T_h . The right side is the cold side and

consists of an array of fins. This side is kept at cold temperature T_2 and the air adjacent to it is at T_c , then the heat transfer through the wall from the hot air to the cold air is expressed as [17]:

$$Q_f = \frac{T_h - T_c}{1/h_i + l/k + \frac{1}{(A_{tot}/A_w)\eta h}} \quad (3.33)$$

Equation (3.33) is applicable to the type of fins (rectangular, pin or trapezoidal)

3.2.5 Estimation of The Fin Dimensions

The fin dimensions of the model that represents the wall texture can be estimated by knowing the volume of the texture material of the stone. This volume is the same as the volume of the array of fins (V_f)

The volume V_f may be found by finding the void volume V_v between the fins. If V_t is the total volume of fins and voids, then

$$V_f = V_t - V_v \quad (3.34)$$

The same applies to fins of irregular shape, such as that of stone walls.

It is known that the stone has a certain length, a certain width and has surface irregularities of a certain thickness. Since the texture has an irregular shape, the void volume (V_v) must be measured experimentally. This volume may be measured using the sand box technique. The sand box is simply a box which has the same dimensions of the stone. The large face is made of glass (Fig. 3.3). The technique simply consists of filling the space of the irregular shape by a very fine sand and then measuring the volume of this sand (Fig. 3.4). This volume is the void volume between the fins (V_v). The total volume (V_t) can be measured from the dimensions of the stone inside the box. i.e. V_t is the total volume of the space between the glass face of the sand box and the straight edge of the stone regardless of the texture. Then the volume of the fin (V_f) can be evaluated using equation (3.34). The fin volume (V_f) gives the total volume of the array of fins and not the volume of a single fin, and since the stones have different dimensions, it is convenient to evaluate the total volume of fins per wall, which means per 1 m^2 (the area of the tested wall). This can be done by the relation:

$$V_f = V_{f(stone)} \times \frac{A_w}{A_s} \quad (3.35)$$

where A_s is the area of single stone. In this case V_f can be evaluated for each stone and then the average volume is to be taken. The dimensions of the fin can now be estimated for each type of fins

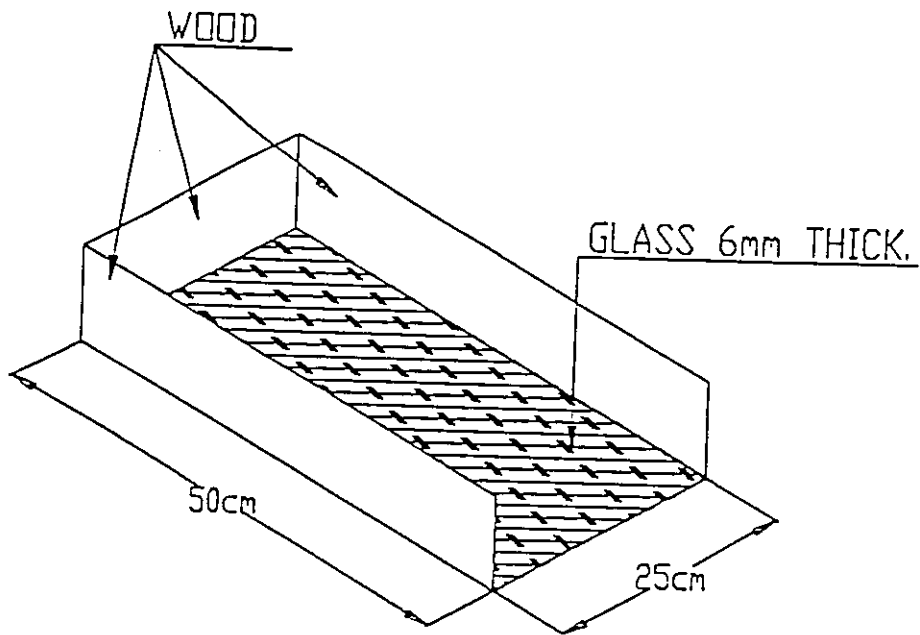


Fig. 3.3: Sand box

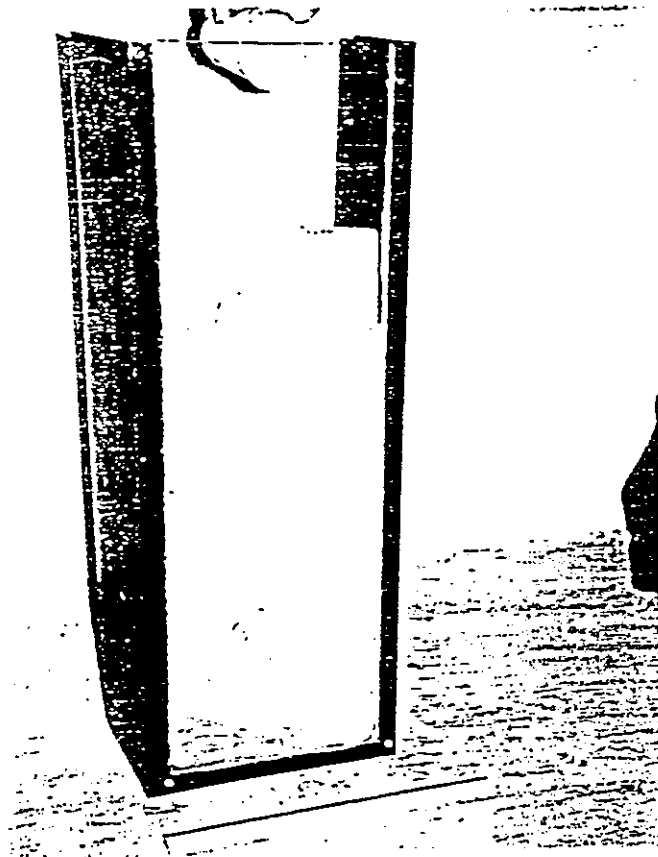


Fig. 3.4: Picture of the sand box

Rectangular Fin

A schematic diagram of the array of rectangular fins is shown in Fig.3.2. The most acceptable specifications of the array of rectangular fins that represent a stone wall is when taking the spacing between the fins to be equal to the width of a single fin, in this case

$$\delta = 2w_r \quad (3.36)$$

the width of a single rectangular fin can be found using the dimensions of the wall. The wall used in the experiments in this work has a dimension of 1m x 1m, and the rectangular fin has a thickness of 1m (along the width of the wall). The width of the fin can be found as follows:

$$\delta = \frac{1}{n} \quad (3.37)$$

and from equation (3.36)

$$w_r = \frac{1}{2n} \quad (3.38)$$

where n is the number of fins of the array. since the width is known, the length of the fin can be computed using the volume of the fins (V_f).The fin volume of an array of rectangular fins can be expressed as:

$$(V_f)_r = w_r L_r n \quad (3.39)$$

Hence the length of a single fin can be evaluated to be

$$L_r = \frac{V_f}{nw_r} \quad (3.40)$$

Pin Fin

The dimensions of the pin fin can be estimated by distributing the fins on the wall in a symmetrical way, i.e. the distance between any two fins is the same. In this case, the number of fins along the length (and the width) of the wall is \sqrt{n} (mathematically expressed). to estimate the dimensions of the fin, the distance between any two fins must be known. If taking this distance to be the same as the diameter of the pin fin (D), then the diameter can be calculated as follows:

$$D = \frac{1}{2\sqrt{n}} \quad (3.41)$$

Now it is easy to find the length of the fin by using the volume of the fins:

$$(V_f)_p = n \frac{\pi D^2}{4} L_p \quad (3.42)$$

and hence the fin length is given by:

$$L_p = \frac{4V_f}{\pi n D^2} \quad (3.43)$$

Trapezoidal Fin:

The array of trapezoidal fins has a distance between the centers of the fins (δ) to be the same as the rectangular fin (equation 3.37) which is applicable for any array of longitudinal fins. The estimation of its dimension can take the approach of the schematic diagram of the trapezoidal fin shown in Fig. 3.1. In this case the width of the trapezoidal fin can be taken as:

$$w_1 = \frac{3}{4}\delta \quad (3.44)$$

The small base of the trapezoidal fin (which can be denoted by w_2) is expressed as

$$w_1 = \frac{1}{4}\delta \quad (3.45)$$

or

$$w_2 = \frac{1}{3}w_1 \quad (3.46)$$

One can take this approach in order to have the volume of the rectangular fin to be the same as the trapezoidal fin. The length of the trapezoidal fin can be computed using the fin volume:

$$(V_f)_t = 2L_t n \left(w_t + \frac{1}{3} w_t \right) \quad (3.47)$$

$$L_t = \frac{V_f}{\frac{2}{3} w_t n} \quad (3.48)$$

noting that the length of the trapezoidal fin in this case is the same as the length of the rectangular fin.

3.2.6 Fin Heat Transfer Rate

By knowing the dimensions of each type of array of fins, the performance of the fin can now be evaluated with the consideration that the wall is a smooth wall and an array of fins is attached to it. The heat transfer rate through the wall can be evaluated using equation (3.49):

$$Q_j = \frac{T_h - T_c}{1/h_i + l/k + (A_{tot}/A_w)_j \eta_j h} \quad (3.49)$$

or in easier way

$$Q_j = \frac{T_h - T_c}{(A_{tot} / A_w)_j \eta_j h} \quad (3.50)$$

where j can take the letters r , p or t denoting for rectangular, pin or trapezoidal array of fins respectively. The value of heat transfer rate calculated from the equation (3.50) is to be compared with the experimental heat - transfer rate taken during the test.

CHAPTER 4

EXPERIMENTAL RIG AND PROCEDURE

4.1 Introduction:

Thermal performance of many walls can be estimated from the conductivities and thicknesses of their components. However, some walls are complicated by the inclusion of structural members, for example, and tests to find their thermal performance become necessary. When dealing with specimens that represent real walls, the problem of evaluating the overall heat - transfer coefficient becomes difficult. The difficulty comes from the fact that an accurate data of the surroundings must be known (see equation 3.1). Furthermore, the heat transfer rate through the wall must be known properly. The solution of this problem is to build an appropriate device in which a real wall must be built between two rooms (Fig. 4.1), one room is set in a constant cold temperature, and the other room has a heat source that gives a known heat rate. In order to assure that all the heat generated in the hot room is transferred to the cold room through the wall, another room of larger size is to be built in which it contains the hot room. The purpose of this room is to artificially make all sides of the test room.

other than that under test, a perfect insulator. This is done by sensing the temperature of the hot room and controlling the temperature between the two rooms to be the same as the temperature of the hot room. In this case it is guaranteed that all the heat input in the hot room is transferred to the wall (which means Q is properly known). On the other hand, the surrounding temperatures of the wall are also well known (T_h and T_c).

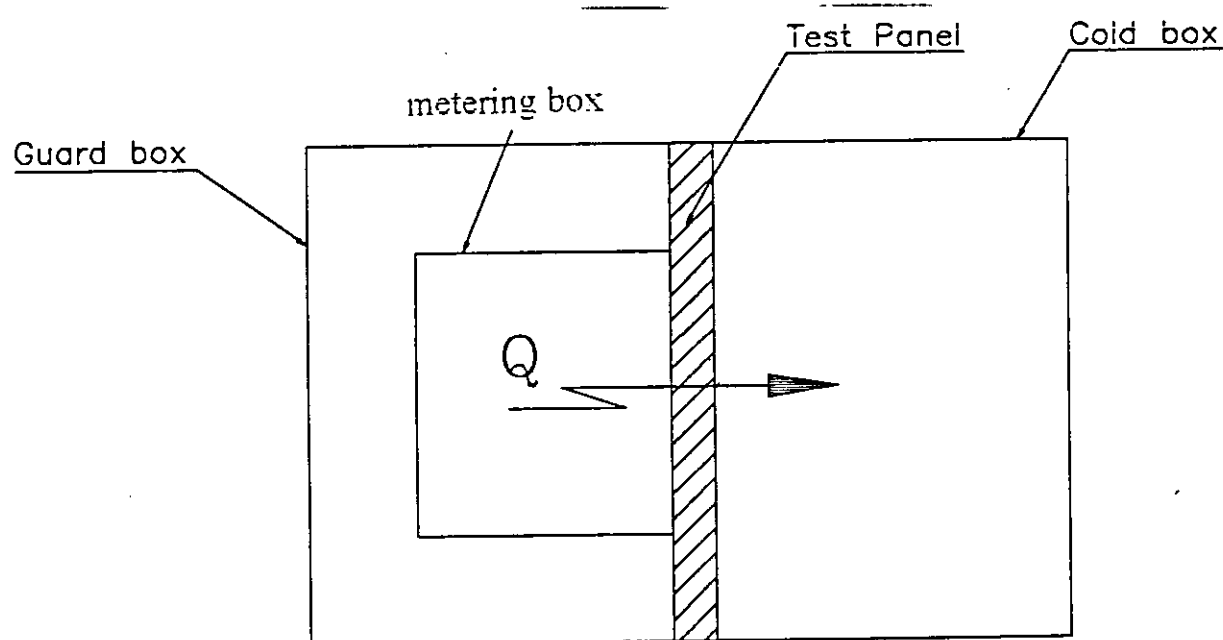


Fig. 4.1: Purpose of the test

The test method accommodates large specimens representing actual construction. The test method known as the guarded hot box method, covers the measurements of steady - state thermal transfer properties of building assemblies. This test method is suitable for building wall, panels, and other applications of non-homogeneous specimens at similar temperature ranges. It may also be used for homogeneous specimens.

4.2 The Apparatus

The guarded hot box is an apparatus designed to determine thermal performance for representative test panels and is an arrangement for establishing and maintaining a desired steady temperature difference across a test panel for the period of time necessary to maintain a constant heat flux and steady temperature, and for an additional period adequate to measure these quantities to the desired accuracy [18]. This test method is considered as a standard test by the ASTM (American Society for Testing and Materials) and designated as C 236 test method.

In general the apparatus consists of three main parts: the metering box, the guarded box and the cold box. Fig. 4.2 shows a schematic

arrangement of the test panel and of the various major elements of the apparatus. Fig. 4.2,b and c shows alternative arrangements. There are other arrangements with the same purpose depending on the application of the panel. In general, the size of the metering box determines the minimum size of the other elements of the test. the schematic diagram of the apparatus used in this work is shown in Fig. 4.3. A picture of the apparatus used in this work is shown in Fig. 4.4.

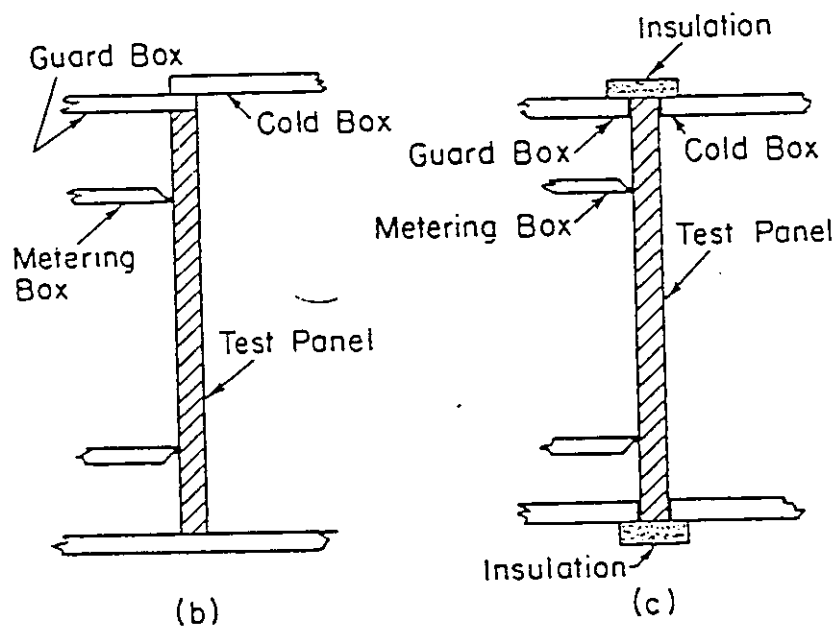
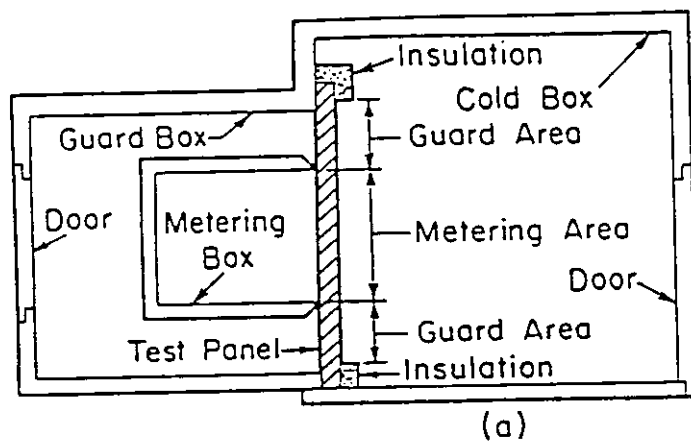


Fig. 4.2: General arrangements of test box, guard box, test panel, and cold box

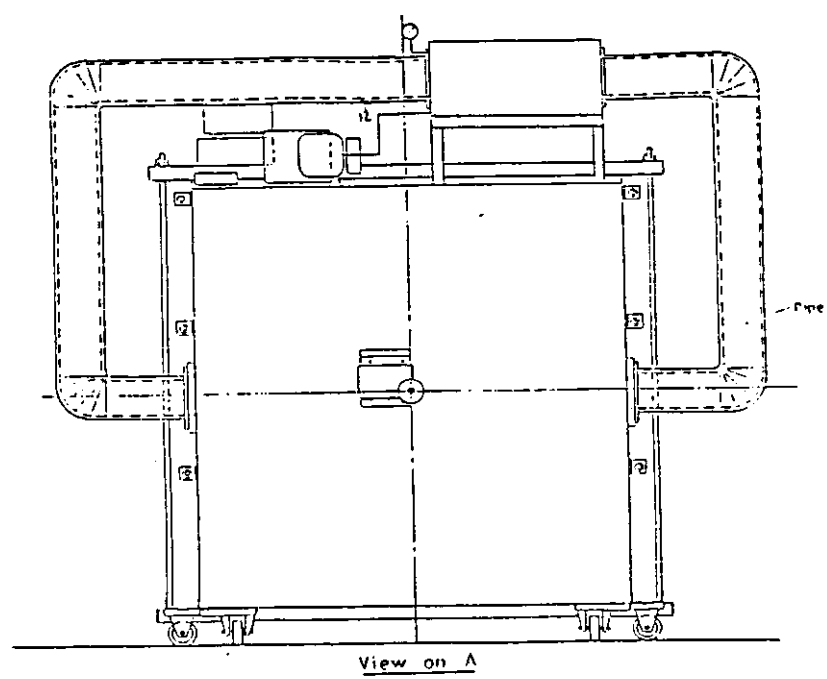
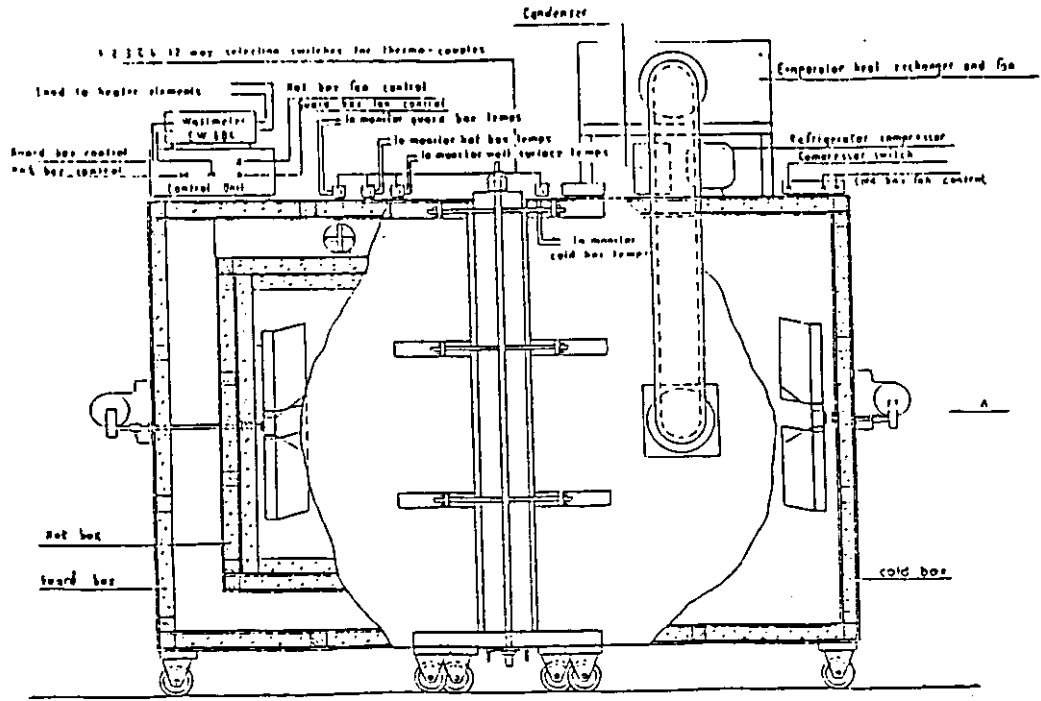


Fig. 4.3: Schematic diagram of the apparatus used in the experiment.

4.3 The metering box

The metering box is the most important part of the apparatus. It has five well-insulated sides and the 6th is its face against the test panel a photograph of this box is shown in Fig. 4.5. The size of the metering box is largely governed by the metering area required to obtain a representative area of the panel. The height of the metering box should not be less than the width. The depth of the metering box should not exceed the space required to occupy the necessary equipments. The apparatus used in this research has a metering box of 1.0 meter height, 1.0 meter width and 1.0 meter depth. It contains an electrical heating element and a fan for air circulation. When the apparatus is used to test panels in a vertical position, the moderate circulation resulting from natural convection is sufficient without the use of a fan as in this research. If the fan is used, its motor should be within the metering box, its electrical input should be as small as possible, and the input should be carefully measured. If it is necessary to locate the motor outside the metering box (as in the apparatus used in this research). The heat equivalent of the shaft power must be accurately measured. In this research, and because the test panels representing vertical walls, the fan in the metering box has not been used, and the natural convection was sufficient and guaranteed.

The heat is supplied to the metering box by means of an electric heater. This heater is controlled manually from the outside of the apparatus. The heat input ranges from 0.0 to 50.0 watt. The contact edges of the metering box ensure (by a rubber gasket) a tight air seal against the hot surface of the test panel. The metering box is pressed tightly against the test panel by steel bolts.

4.4 The Guard Box

The guard box is a five wall enclosure with its face against the test sample. This face is called the hot face. It is larger than the metering box and the metering box is completely inside the guard box. This box is shown in the same photograph showing the metering box (Fig. 4.5). The main purpose of the guard box is to ensure that there is no heat escape from the metering box to the surrounding and all the heat supplied to the metering box is transferred to the test panel. The dimensions of the guard box is 156 cm length, 156 cm width and 125 cm depth. It contains four small fans located in the area between the metering box and the guard box : one above, one under and two at the sides. The purpose of these fans is to circulate the air between the metering box and the guard box to ensure that this space has the

same temperature. Also in this space a differential heater is located. This heater detects the temperature of the metering box and controls the temperature of the space between the metering box and the guard box to be the same as that of the metering box. In this way, it is ensured that the hot box (guard box and metering box) has the same temperature, and hence the heat transferred between them is zero. As a result, all the heat supplied to the metering box is transferred to the test panel.

4.5 The Cold Box

The cold box is a five wall enclosure and its face is against the test panel facing the opposite side of the hot surface. This surface is the cold surface. A photograph of the box is shown in Fig. 4.5. This box is kept cold (at a controlled cold temperature) by means of a refrigerating unit. The purpose of the cold box is to keep the cold box at a constant (low) temperature, so that it becomes like the outside condition of the tested wall.

The size of the cold box is governed by the size of the test panel or by the arrangement of the boxes used. Its dimensions in this work are: 156 cm length, 156 cm width and 102 cm depth. The cold box is heavily insulated.

The function of the insulation is just to reduce the required refrigerating capacity. The refrigerating unit is installed above the cold box and the cold air is supplied to the box by means of a duct and two small fans, one at each side of the cold box. The evaporator is located inside the duct above the cold box. A large fan similar to a ceiling fan is fixed at the centre of the back wall of the cold box. The speed of this fan is controlled from outside and has five different speeds. The fan has two functions: first, is to circulate the air inside the cold box, and second to show the effect of different air velocities on the heat transfer coefficient.

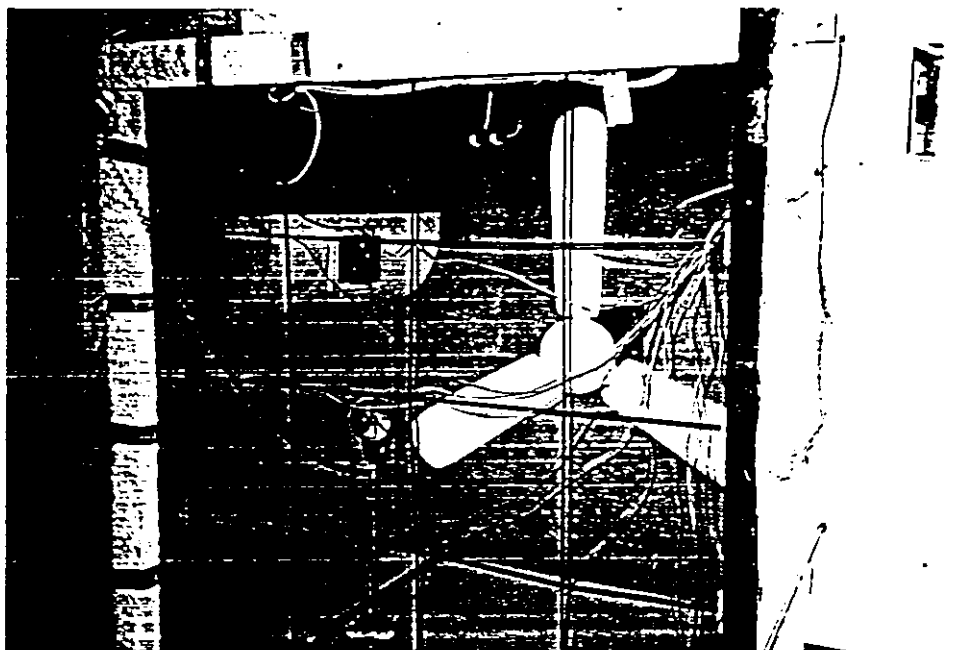


Fig. 4.6: A photograph of the cold box

4.6 The Sample Frame

The sample frame is a rigid frame made of steel and has the same length and width of the two main boxes. A photograph of the frame is shown in Fig.4.7. The frame can be moved by means of four wheels. The thickness of the frame is 10 cm, thereby allowing the test of walls and panels of approximately similar thickness.



Fig. 4.7: A photograph of the sample frame

4.7 Measuring devices

The variables that were measured during the experiments are: temperature, heat input and air velocity. Temperature and heat input read outs are taken by instruments shown in the photograph, Fig. 4.8.

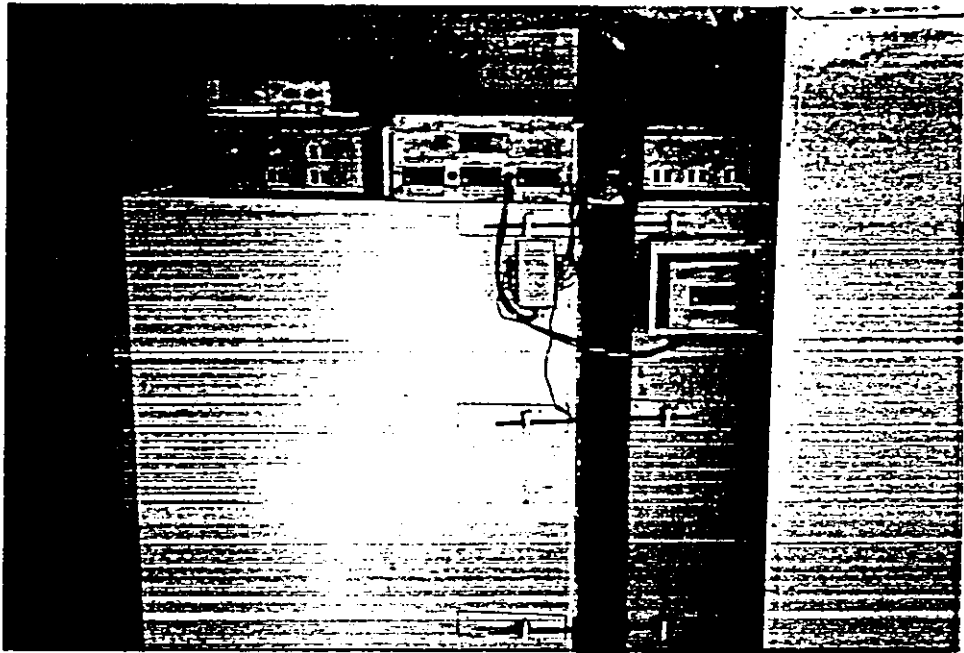


Fig. 4.8: A photograph showing the instruments of temperature and heat input read outs

4.7.1 Temperature Measurement:

Temperatures were measured using copper - constant (type T) thermocouples along with a digital read out with 12 selector switch. A measurement grid is available 5 mm away from each side of the wall and

each grid is provided with nine measuring points. These two grids were used to measure the air temperature. In addition, surface temperatures are taken for five points fixed at the hot surface, five points fixed at the cold surface and three points at various locations in the space between the metering box and the guard box. The temperatures measured are:

1. Hot room temperature (T_h) averaged from the nine points.
2. Cold room temperature (T_c) averaged from the nine points.
3. Hot surface temperature (T_1) averaged from the five points.
4. Cold surface temperature (T_2) averaged from the five points.
5. Guard box temperature (T_g) averaged from the three points.

4.7.2 Heat Input Measurement:

The heat input to the metering box is measured using a watt-meter. This device measures the electric power consumed by the DC electric heater and is also controlled from outside the box.

In general, the hot box has a temperature control circuit which can supply up to 50 watt into a 10 Ω heater elements at temperatures in the range 20 $^{\circ}\text{C}$ to 40 $^{\circ}\text{C}$. The output from the heater control circuit is direct

current (DC) which can be measured by an electronic watt-meter to indicate the power input to the heater. The watt-meter is made by Feed Back Ltd. Type EW 604. The Guard Box temperature control uses a differential temperature measurement system which causes the guard box to track the temperature of the hot box.

4.7.3 Air Velocity Measurement:

The air velocity of the cold room is controlled by a fan switch. The air movement of the cold room simulates of the outside wind blowing on the building . It is measured using a propeller vane anemometer.

4.8 Experimental Work Procedure

The test method called the guarded hot box method, is primary designed for the temperatures encountered in normal building use, however it is recognized that the method may find application in testing conditions that are outside this normal range.

The experimental work in this research was divided into four similar experiments. Each experiment is concerned with a different type of wall. The first deals with the smooth-surface stone wall, the second deals with the hammered “Musamsam” stone wall, the third deals with the punched “Mufajjar” stone wall and finally the fourth experiment deals with the rough-surface “Tubzeh” stone wall. Each stage takes the following steps:

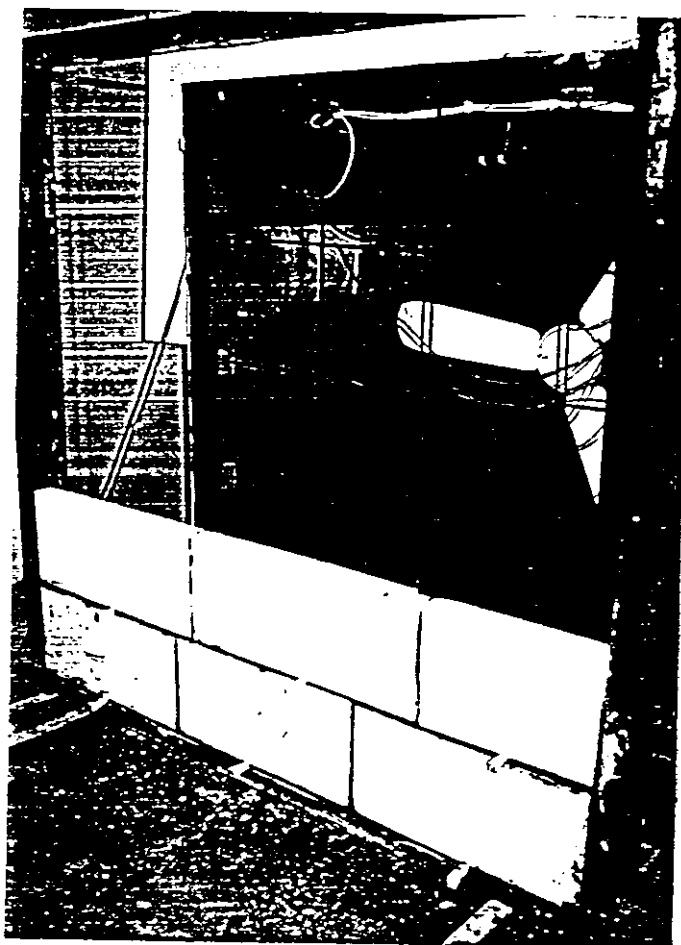


Fig. 4.9: Building up the wall inside the frame

- The first step is building up the wall inside the frame (Fig. 4.9). The wall is built so that its face is against the cold box and its back is against the hot box in a manner that it represents an actual wall in the winter. The size of the wall is 156 cm length, 156 width and 5 cm thickness. The stones of the wall were constructed together using cement and sand with ratio of 2:1 sand to cement.
- The second step is to fix five of the thermocouples at the hot surface (as shown in the photograph, Fig. 4.10), and five at the cold surface and exactly opposite to the hot surface ones.



Fig. 4.10: A photograph showing the thermocouples fixed on the wall

- The wall is fixed tightly in its place between the two main boxes by means of steel bolts as shown previously in Fig. 4.8, and the refrigerating unit is operated with its thermostat setting as low as possible. The heater in the metering box is also switched on, the maximum power input in this work was 48 watt, and was arbitrary selected to be the same in all experiments. The fan in the cold box is switched on and the speed of the fan is set at a specific speed.
- The test conditions are maintained until substantially constant temperatures and heat flow readings are attained
- After a steady state is achieved, and as recommended by ASTM C-236, the test period is continued at least 8 hours after which two or more successive four-hour period tests produce results that do not differ by more than 1% [17]. During this period, data is taken at intervals of one hour or less. The average of the data for the two or more successive four-hour periods that agree within 1% are used in calculating the final results.
- The data that are taken during the experiments are the hot surface temperatures (five readings), the cold surface temperature (five readings), the metering box temperature (nine readings), the cold box temperature (nine readings) and the guard box temperature (three readings). To achieve steady state these readings must be constant. The other data

(heat input and air velocity) are input data and does not affect on the steady-state condition.

- Once the test at a certain hot room temperature is completed, the test is repeated at various hot room temperatures within a reasonable range, say 16 - 28°C.

CHAPTER 5

DATA AND CALCULATIONS

The detailed data taken during the experiment is included in Appendix A. Each table represents one required parameter. The data shown below is the average values :

5.1 Experimental Results

The following tables show the experimental results of this work, and the temperatures used in the tables are the average values of the temperatures listed in Appendix A

Table 5.1: Result for smooth-surface wall ($v = 1.6$ m/s, $h_{th} = 11.86$ W/(m².C))

No.	Q (W)	T _h (°C)	T ₁ (°C)	T ₂ (°C)	T _c (°C)	k W/(m.C)	U W/(m ² .C)	h W/(m ² .C)
1	48	16	13	12	6	2.4	4.8	8
2	48	18	15	14	8	2.4	4.8	8
3	48	20	17	16	10	2.4	4.8	8
4	48	22	19	18	12	2.4	4.8	8
5	48	24	21	20	14	2.4	4.8	8
6	48	26	23	22	16	2.4	4.8	8
7	48	28	25	24	18	2.4	4.8	8

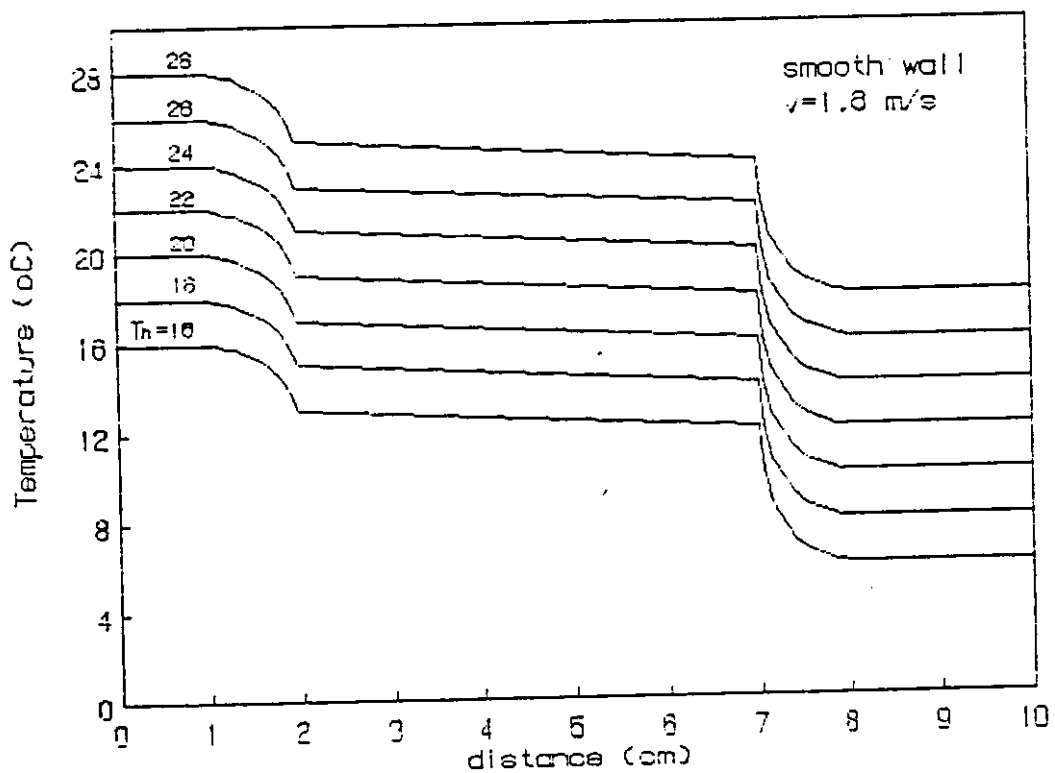


Fig. 5.1: Temperature distribution through smooth wall ($v = 1.6$ m/s)

Table 5.2: Result for Smooth - surface wall ($v = 0.5$ m/s, $h_{th} = 7.57$ W/(m².C))

No.	Q (W)	T _h (°C)	T ₁ (°C)	T ₂ (°C)	T _c (°C)	k W/(m.C)	U W/(m ² .C)	h W/(m ² .C)
1	48	16	11	10	2	2.4	3.43	6
2	48	18	13	12	4	2.4	3.43	6
3	48	20	15	14	6	2.4	3.43	6
4	48	22	17	16	8	2.4	3.43	6
5	48	24	19	18	10	2.4	3.43	6
6	48	26	21	20	12	2.4	3.43	6
7	48	28	23	22	14	2.4	3.43	6

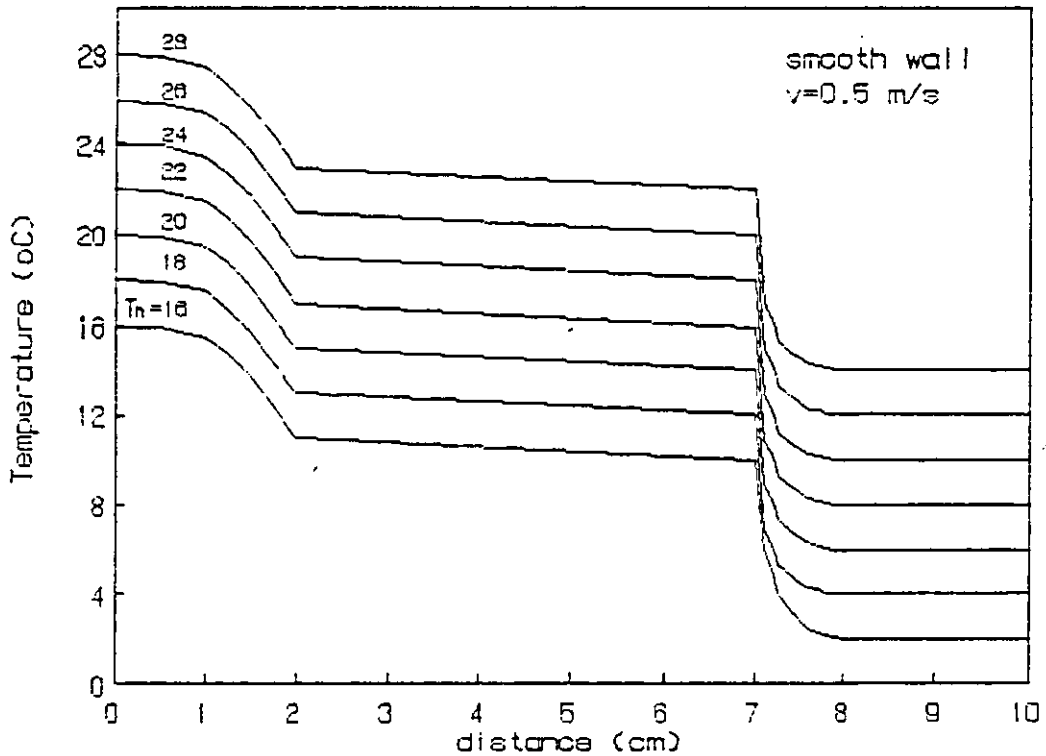


Fig. 5.2: Temperature distribution through smooth wall ($v = 0.5$ m/s)

Table 5.4 Result for Hammered wall ($v = 0.5$ m/s, $h_{th} = 7.57$ W/(m².C))

No.	Q (W)	T _h (°C)	T ₁ (°C)	T ₂ (°C)	T _c (°C)	k W/(m.C)	U W/(m ² .C)	h W/(m ² .C)
1	48	16	11	10	3	2.4	3.69	6.87
2	48	18	13	12	5	2.4	3.69	6.87
3	48	20	15	14	7	2.4	3.69	6.87
4	48	22	17	16	9	2.4	3.69	6.87
5	48	24	19	18	11	2.4	3.69	6.87
6	48	26	21	20	13	2.4	3.69	6.87
7	48	28	23	22	15	2.4	3.69	6.87

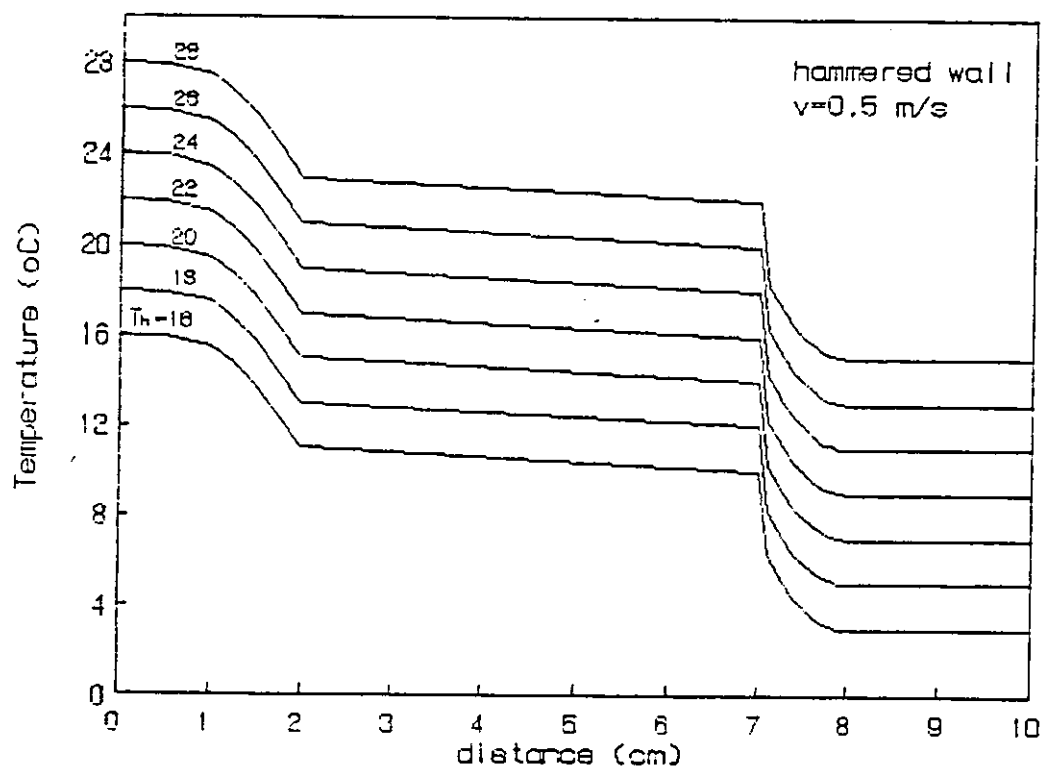
Fig. 5.4: Temperature distribution through hammered wall ($v=0.5$ m/s)

Table 5.5 Result for Punched wall ($v = 1.6$ m/s, $h_{th} = 11.86$ W/(m².C))

No.	Q (W)	T _h (°C)	T ₁ (°C)	T ₂ (°C)	T _c (°C)	k W/(m.C)	U W/(m ² .C)	h W/(m ² .C)
1	48	16	13	12	8	2.4	6	12
2	48	18	15	14	10	2.4	6	12
3	48	20	17	16	12	2.4	6	12
4	48	22	19	18	14	2.4	6	12
5	48	24	21	20	16	2.4	6	12
6	48	26	23	22	18	2.4	6	12
7	48	28	25	24	20	2.4	6	12

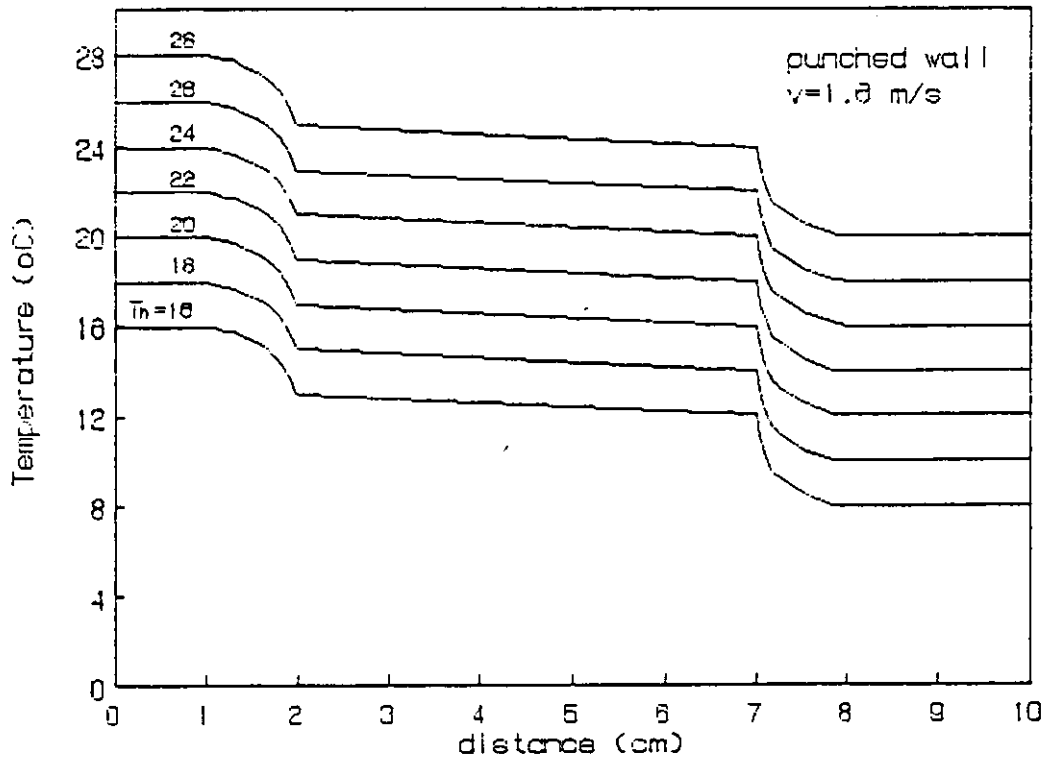


Fig. 5.5: Temperature distribution through punched wall ($v = 1.6$ m/s)

Table 5.6 Result for Punched wall ($v = 0.5 \text{ m/s}$, $h_{th} = 7.57 \text{ W/(m}^2\cdot\text{C)}$)

No.	Q (W)	T_h ($^{\circ}\text{C}$)	T_1 ($^{\circ}\text{C}$)	T_2 ($^{\circ}\text{C}$)	T_c ($^{\circ}\text{C}$)	k W/(m.C)	U W/(m ² .C)	h W/(m ² .C)
1	48	16	13	12	7	2.4	5.33	9.6
2	48	18	15	14	9	2.4	5.33	9.6
3	48	20	17	16	11	2.4	5.33	9.6
4	48	22	19	18	13	2.4	5.33	9.6
5	48	24	21	20	15	2.4	5.33	9.6
6	48	26	23	22	17	2.4	5.33	9.6
7	48	28	25	24	19	2.4	5.33	9.6

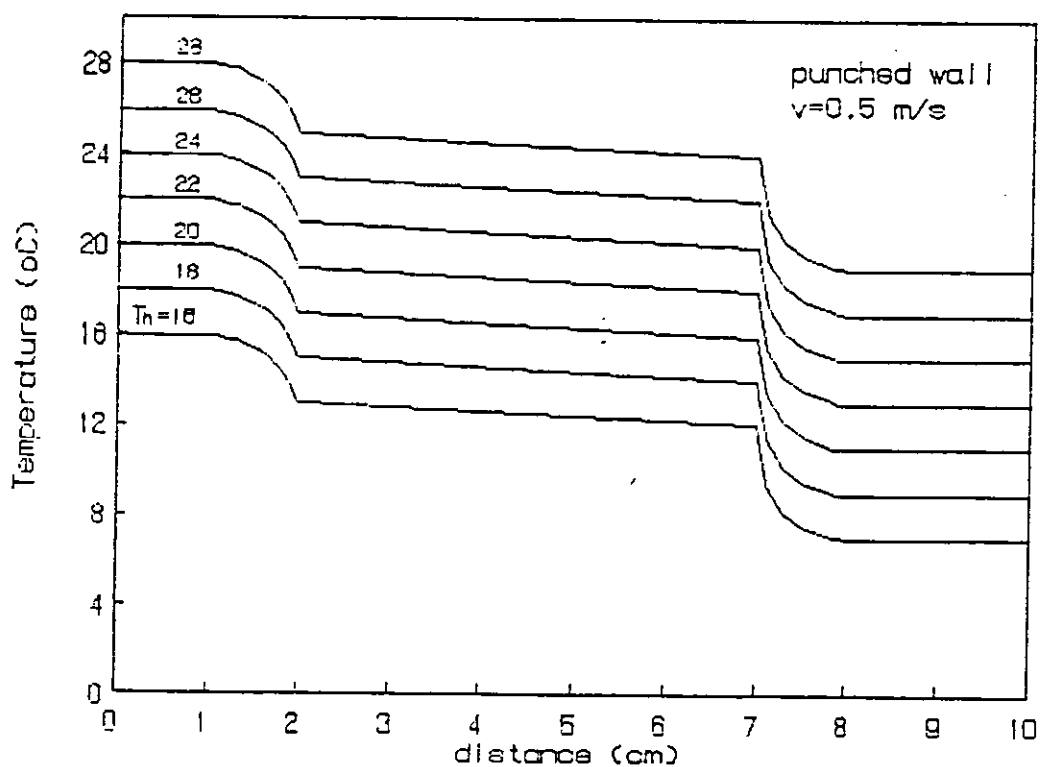
Fig. 5.6: Temperature distribution through punched wall ($v = 0.5 \text{ m/s}$)

Table 5.7: Result for Rough - surface wall ($v = 1.6$ m/s, $h_{th} = 11.86$ W/(m².C))

No.	Q (W)	T _h (°C)	T ₁ (°C)	T ₂ (°C)	T _c (°C)	k W/(m.C)	U W/(m ² .C)	h W/(m ² .C)
1	48	16	13	12	9	2.4	6.86	16
2	48	18	15	14	11	2.4	6.86	16
3	48	20	17	16	13	2.4	6.86	16
4	48	22	19	18	15	2.4	6.86	16
5	48	24	21	20	17	2.4	6.86	16
6	48	26	23	22	19	2.4	6.86	16
7	48	28	25	24	21	2.4	6.86	16

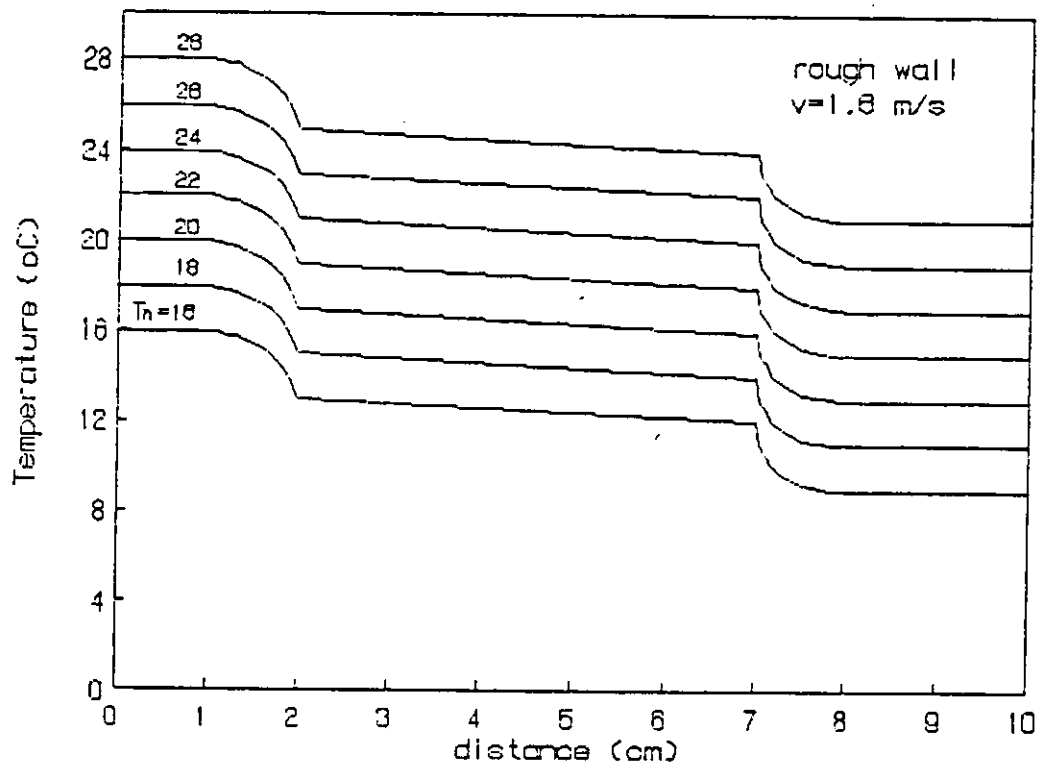


Fig. 5.7: Temperature distribution through rough wall ($v = 1.6$ m/s)

Table 5.8 Result for Rough - surface wall ($v = 0.5$ m/s, $h_{th} = 7.57$ W/(m².C))

No.	Q (w)	T _h (°C)	T ₁ (°C)	T ₂ (°C)	T _c (°C)	k W/(m.C)	U W/(m ² .C)	h W/(m ² .C)
1	48	16	13	12	8	2.4	6	12
2	48	18	15	14	10	2.4	6	12
3	48	20	17	16	12	2.4	6	12
4	48	22	19	18	14	2.4	6	12
5	48	24	21	20	16	2.4	6	12
6	48	26	23	22	18	2.4	6	12
7	48	28	25	24	20	2.4	6	12

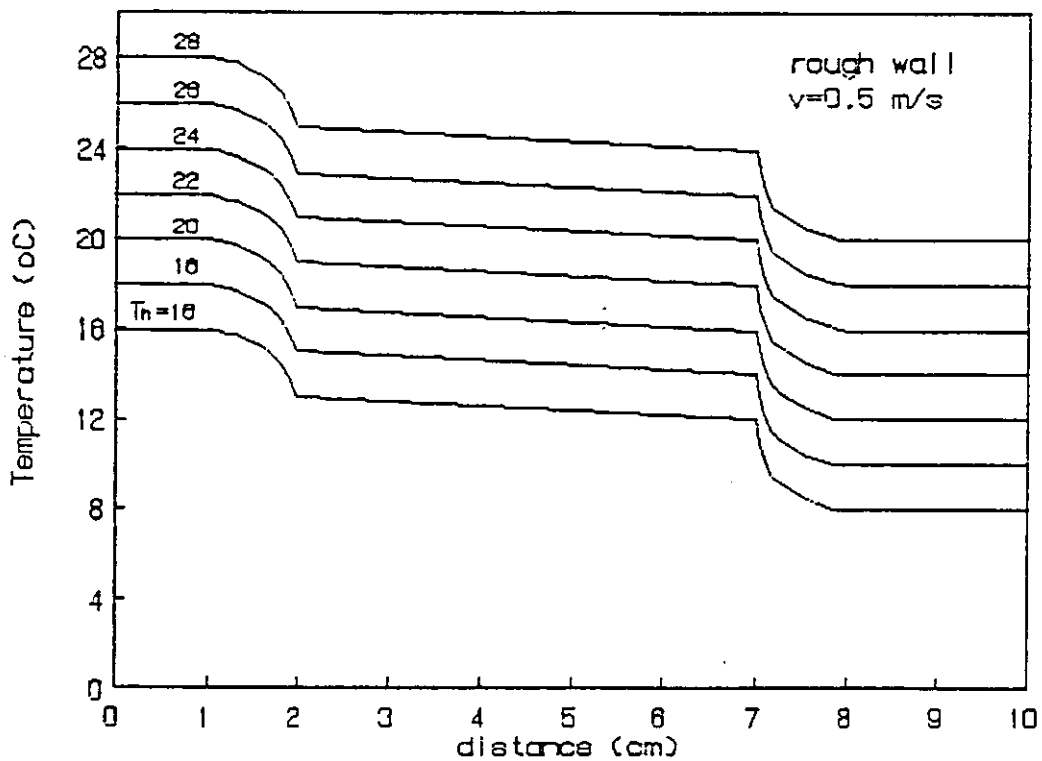


Fig. 5.8: Temperature distribution through rough wall ($v = 0.5$ m/s)

5.2 Error Analysis

Error analysis of the experimental results can be summarised in this section. The uncertainty of each experimental parameter is summarised in table 5.9 below which shows uncertainty in the measurements of the three basic parameters taken in the experimental work. These parameters are: the heat transfer rate (Q), the length (l), and the temperature (T):

Table 5.9: Uncertainties in the basic measurements (Q, l and T)

Parameter	Instrument	Smallest reading	Uncertainty
Q=48 W	Wattmeter	1 W	$\Delta Q = \pm 0.5 \text{ W}$ $\Delta Q/Q = \pm 1.042 \%$
l = 0.05 m	meter	0.001 m	$\Delta l = \pm 0.0005 \text{ m}$ $\Delta l/l = \pm 1 \%$
T	Thermocouple	1 °C	$\Delta T = \pm 0.5 \text{ °C}$

The uncertainties mentioned in table 5.9 are based on the half of the smallest reading of each instrument. Based on these values the uncertainties of calculated parameters can be evaluated as follows:

The area of the wall is $A = 1\text{m}^2$ comes from the multiplication of the length of the wall (1 m) and the width of the wall (1 m), hence the uncertainty of the area is given by:

$$\Delta A/A = (2)^{1/2} (\pm 0.0005) \quad (5.1)$$

$$\Delta A/A = \pm 0.0707 \% \quad (5.2)$$

Error of calculating U, h and k:

Let:

$$Y_U = T_h - T_c \quad (5.3)$$

$$Y_h = T_2 - T_c \quad (5.4)$$

$$Y_k = T_1 - T_2 \quad (5.5)$$

Then the uncertainties of the Y's can be expressed as:

$$\Delta Y_U = [(\Delta T_h)^2 + (\Delta T_c)^2]^{0.5} \quad (5.6)$$

$$\Delta Y_h = [(\Delta T_2)^2 + (\Delta T_c)^2]^{0.5} \quad (5.7)$$

$$\Delta Y_k = [(\Delta T_1)^2 + (\Delta T_2)^2]^{0.5} \quad (5.8)$$

The values of ΔY depends only on ΔT which is ± 0.5 °C, and hence $\Delta Y = \pm 0.707$ °C for all the values of the equations 5.6 to 5.8. In order to find the errors associated to U, h, and k equations 3.1 to 3.3 are rewritten as follows:

$$U = \frac{Q}{AY_U} \quad (5.9)$$

$$k = \frac{Ql}{AY_k} \quad (5.10)$$

$$h = \frac{Q}{AY_h} \quad (5.11)$$

Hence, by using equations 5.9 to 5.11 the error corresponding to U, k, and h can be expressed as follows

$$\frac{\Delta U}{U} = \pm \left[\left(\frac{\Delta Q}{Q} \right)^2 + \left(\frac{\Delta A}{A} \right)^2 + \left(\frac{\Delta Y_U}{Y_U} \right)^2 \right]^{1/2} \quad (5.12)$$

$$\frac{\Delta k}{k} = \pm \left[\left(\frac{\Delta Q}{Q} \right)^2 + \left(\frac{\Delta l}{l} \right)^2 + \left(\frac{\Delta A}{A} \right)^2 + \left(\frac{\Delta Y_k}{Y_k} \right)^2 \right]^{1/2} \quad (5.13)$$

$$\frac{\Delta h}{h} = \pm \left[\left(\frac{\Delta Q}{Q} \right)^2 + \left(\frac{\Delta A}{A} \right)^2 + \left(\frac{\Delta Y_h}{Y_h} \right)^2 \right]^{1/2} \quad (5.14)$$

using table 5.9 and equation 5.2, equations 5.12 to 5.14 can be rewritten as:

$$\frac{\Delta U}{U} = \pm \left[1585 + \left(\frac{\Delta Y_U}{Y_U} \right)^2 \right]^{1/2} \quad (5.15)$$

$$\frac{\Delta k}{k} = \pm \left[1595 + \left(\frac{\Delta Y_k}{Y_k} \right)^2 \right]^{1/2} \quad (5.16)$$

$$\frac{\Delta h}{h} = \pm \left[1585 + \left(\frac{\Delta Y_h}{Y_h} \right)^2 \right]^{1/2} \quad (5.17)$$

Procedure:

- The values of U , k and h that are used for calculating the error are the values in tables 5.1 to 5.8.
- Y is calculated using equations 5.3 to 5.5, and the temperatures are taken from tables 5.1 to 5.8.
- Y is calculated using equations 5.6 to 5.8.
- Errors are computed using equations 5.15 to 5.17.

From the previous analysis, it is noticed that the error associated with U , k and h depends on the value of Y , which is a temperature difference. From tables 5.1 to 5.8 it can be noticed that for each table, Y is constant, and hence the error of U , k and h is constant for each table. The results of the error evaluation can be listed in the tables below:

Table 5.10: Uncertainties in the measurements of U, k and h ($v = 0.5$ m/s)

Wall type	U (W/m ² .C)	k (W/m.C)	h (W/m ² .C)	ΔU (W/m ² .C)	Δk (W/m.C)	Δh (W/m ² .C)	$\Delta U/U$ (%)	$\Delta k/k$ (%)	ΔZ (%)
smooth	3.43	2.4	6.0	± 0.17	± 0.46	± 0.53	± 5.16	± 19	± 8.89
hammered	3.69	2.4	6.87	± 0.20	± 0.46	± 0.69	± 5.54	± 19	± 10.1
punched	5.33	2.4	9.6	± 0.42	± 0.46	± 1.10	± 7.92	± 19	± 11.4
rough	6.0	2.4	12.0	± 0.53	± 0.46	± 1.41	± 8.89	± 19	± 11.7

Table 5.11: Uncertainties in the measurements of U, k and h ($v = 1.6$ m/s)

Wall type	U (W/m ² .C)	k (W/m.C)	h (W/m ² .C)	ΔU (W/m ² .C)	Δk (W/m.C)	Δh (W/m ² .C)	$\Delta U/U$ (%)	$\Delta k/k$ (%)	$\Delta h/h$ (%)
smooth	4.8	2.4	8.00	± 0.34	± 0.46	± 0.82	± 7.18	± 19	± 10.2
hammered	5.33	2.4	9.60	± 0.42	± 0.46	± 1.05	± 7.95	± 19	± 10.9
punched	6.00	2.4	12.0	± 0.53	± 0.46	± 1.29	± 8.90	± 19	± 10.8
rough	6.86	2.4	16.0	± 0.69	± 0.46	± 2.00	± 10.2	± 19	± 12.5

5.3 Fin Model Results

The fin model is explained theoretically in chapter 3, but here, the results of this model are explained and presented. First of all, the number of fins that represent each type of stone is determined. This can be done by noticing the average number of the domes of one stone. For each type of stones the number of domes is to be extended to represent the whole wall, then the average value is taken for all stones of the same type, this number is the number of fins per wall (1 m^2). In the same manner, the volume of the fins is measured using the sand box technique which measures the void volume, and then the fin volume is measured using the relation (3.34). The results are tabulated in table 5.12

Table 5.12: Estimation of the number of fins and volumes of the walls

wall type	no. of fins (n)	void volume (cm ³)	total volume (cm ³)	fin volume (cm ³)
hammered	400	722.20	1000	297.15
punched	120	7484.70	10000	2515.30
rough	18	29400	500000	20600

Since V_f and n are known, the dimensions of fins can be evaluated as explained in the previous chapter. For each type of the wall, there are three types of fin models, and each type has its own dimensions. The results of fin dimension measurements are tabulated in the following tables(5.13 to 5.15):

Table 5.13: Fin dimensions for rectangular fin model

wall type	w_r (mm)	L_r (mm)
hammered	1.25	0.594
punched	4.167	5.033
rough	27.78	41.20

Table 5.14: Fin dimensions for pin fin model

wall type	D_p (mm)	L_p (mm)
hammered	25.00	1.51
punched	45.64	12.82
rough	117.85	104.97

Table 5.15: Fin dimensions for trapezoidal fin model

wall type	w_t (mm)	L_t (mm)
hammered	1.87	0.59
punched	6.25	5.03
rough	41.67	41.20

Model Heat Flow Rate:

One can theoretically evaluate the heat flow rate of the fin models using the following steps for each type of fin where the number of fins is taken from table 5.12 together with the fin volume of the array for each wall type:

-Rectangular Fin:

1. From table 5.13, w_r and L_r are taken for each wall type.
2. P_r and A_r are computed using equations (3.7) and (3.8) respectively.
3. m is computed using equation (3.6).
4. Fin effectiveness (ϕ_r) is calculated using equation (3.17).
5. The ratio $(A_f/A_{tot})_r$ is computed using equation (3.25) taking into consideration that $\delta = 2w_r$
6. The total surface temperature effectiveness (η_r) is computed using equation (3.21)
7. Finally the heat flow rate (Q_r) is computed using equation (3.33).
8. Steps 1 to 7 are repeated for hammered, punched and rough walls.

-Pin Fin:

1. From table 5.14, D and L_p are taken for each wall type.
2. P_p and A_p are computed using equations (3.7) and (3.8) respectively.
3. m is computed using equation (3.6).
4. Fin effectiveness (ϕ_p) is calculated using equation (3.19).
5. The ratio $(A_f/A_{tot})_p$ is computed using equations (3.30) and (3.32)

6. The total surface temperature effectiveness (η_p) is computed using equation (3.21)
7. Finally the heat flow rate (Q_p) is computed using equation (3.33).
8. Steps 1 to 7 are repeated for hammered, punched and rough walls.

-Trapezoidal Fin:

1. From table 5.14, w_t and L_t are taken for each wall type.
2. the parameter f is computed from equation (3.15)
3. R is computed from equation (3.14)
4. Fin effectiveness (ϕ_t) is calculated using equation (3.18).
5. The ratio $(A_f/A_{tot})_t$ is computed using equations (3.29).
6. The total surface temperature effectiveness (η_t) is computed using equation (3.21)
7. Finally the heat flow rate (Q_t) is computed using equation (3.33).
8. Steps 1 to 7 are repeated for hammered, punched and rough walls.

According to the above steps the results are tabulated in table 5.16 which shows the theoretically evaluated (model) heat transfer rate for various wall types and using various fin models.

Table 5.16: Theoretically evaluated (model) heat transfer rate

wall type	Q _r		Q _p		Q _t	
	v=.05 m/s	v=1.6 m/s	v=.05 m/s	v=1.6 m/s	v=.05 m/s	v=1.6 m/s
hammered	54.623	53.543	45.756	44.407	56.787	55.798
punched	56.45	56.918	40.825	42.940	53.254	54.127
rough	51.336	50.365	41.078	41.295	47.996	47.438

Heat - Transfer Coefficients:

According to the results of the fin model, the heat transfer rate obtained from the model can now be used instead of the experimental value in order to obtain the heat transfer coefficients. For each wall type and for each wind speed, the temperature difference between any two points is the same for all of the seven tests. This temperature difference is used in calculating U and h for the model. That is

$$U_{\text{mod}} = \frac{Q_{\text{mod}}}{T_h - T_c} \quad (5.1)$$

$$h_{\text{mod}} = \frac{Q_{\text{mod}}}{T_2 - T_c} \quad (5.2)$$

The results are tabulated in tables 5.17 and 5.18 which show theoretically evaluated (model) convective heat transfer and overall heat transfer coefficients for various wall types and using various fin models.

Table 5.17: Theoretically evaluated (model) convective heat-transfer coefficient

wall type	h_r		h_p		h_t	
	$v=0.05$ m/s	$v=1.6$ m/s	$v=0.05$ m/s	$v=1.6$ m/s	$v=0.05$ m/s	$v=1.6$ m/s
hammered	7.80	10.71	6.54	8.88	8.11	11.16
punched	11.29	14.23	8.16	10.73	10.65	13.53
rough	12.83	16.78	10.27	13.765	11.999	15.82

Table 5.18: Theoretically evaluated (model) overall heat-transfer coefficients

wall type	U_r		U_p		U_t	
	$v=0.05$ m/s	$v=1.6$ m/s	$v=0.05$ m/s	$v=1.6$ m/s	$v=0.05$ m/s	$v=1.6$ m/s
hammered	4.20	5.95	3.52	4.93	8.11	11.16
punched	6.27	7.12	4.54	5.37	5.92	6.77
rough	6.42	7.19	5.13	5.90	6.0	6.78

CHAPTER 6

DISCUSSION

6.1 Introduction

The experimental results obtained in this work are generally in good agreement with theoretical prediction. This also agrees well with previous works which support the fact that there is a significant effect for surface texture on heat transfer phenomena as summarized previously in the literature survey.

6.2 Effect of Surface Texture:

From tables 5.1 to 5.8, it is noticed that the overall heat-transfer coefficient and the convective heat transfer coefficient of the cold room are dependent of the wall type. and since all the walls are made of the same material, the heat transfer coefficients depend on the wall texture or roughness.

Each wall type possesses a certain degree of roughness. The degree of roughness has its lowest value for the hammered-surface stone, and has a larger value for the punched stone, and its highest value is for the rough-surface wall. The effect of surface texture of the wall is summarized in table 6.1 below.

Table 6.1: The relation between the type of the wall and heat-transfer coefficients

Wall type	$v = 1.6 \text{ m/s}$		$v = 0.5 \text{ m/s}$	
	U ($\text{W}/\text{m}^2\text{ }^\circ\text{C}$)	h ($\text{W}/\text{m}^2\text{ }^\circ\text{C}$)	U ($\text{W}/\text{m}^2\text{ }^\circ\text{C}$)	h ($\text{W}/\text{m}^2\text{ }^\circ\text{C}$)
Smooth	4.80	8.00	3.43	6.00
Hammered	5.33	9.60	3.69	6.87
Punched	6.00	12.00	5.33	9.60
Rough	6.86	16.00	6.00	12.00

From the above table it is clear that the heat-transfer coefficients increase with the roughness of the wall.

It is known that the value of the heat-transfer coefficient depends upon a variety of factors such as wind speed, air density, viscosity, thermal conductivity, specific heat and geometry of the surface. In this research all of these factors are kept constant except the geometry of the wall surface and the wind speed, which means that the change of the heat transfer coefficient depends only on the surface texture and wind speed. It worths here to note that for each wall, the experiment is carried out for 7 different steady-state conditions, and for each condition, the values of the overall heat-transfer coefficient and the convective heat-transfer coefficient remained constant. This confirms that for each wall type (texture), there is only one value of the overall heat-transfer coefficient and of the convective heat-transfer coefficient.

Although all the temperatures were changed during the 7 tests of each wall, this does not affect on the heat transfer coefficients. This is so because the state in the cold room is forced convection which means that the velocity is the only parameter that affect on the value of h and T (equation 3.4).

6.3 Effect of Wind Speed

Another important factor that affects heat transfer is wind speed. The experimental results that show this effect can be summarized in table 6.2 below:

Table 6.2: The relation between the wind speed and heat transfer.

Wind Speed m / sec	Smooth		Hammered		Punched		Rough	
	U	h	U	h	U	h	h	h
	(W / m ² C)		(W / m ² C)		(W / m ² C)		(W / m ² C)	
0.5	3.43	6.0	3.69	6.87	5.33	9.6	6.0	12.0
1.6	4.8	8.0	5.33	9.6	6.0	12.0	6.87	16.0

From table 6.2, it is obviously noticed that the heat-transfer coefficients (overall and convective) depend on wind speed. That is to say, as the wind speed increases, the heat-transfer coefficient increases.

The theoretical values of the convective heat-transfer coefficient for walls in general are as shown in table 6.3

Table 6.3: Theoretical values of h (all walls)

Wind Speed m / sec	h_{th} (W / m ² °C)
0.5	7.57
1.6	11.86

These values are based on the correlation made by ASHRAE (equation 3.4), the equation implies that the convective heat-transfer coefficient is only velocity dependent. The experimental values do not agree perfectly with the theoretical ones. The reason is that the correlation does not take into consideration the surface texture of the wall. On the other hand, the experimental values of h for both air speeds lie between the minimum and the maximum experimental values.

The equation of the convective heat transfer coefficient (equation 3.4) shows that the relation between h and v is linear. In this research the relation may be linear for each type of stone wall but for each type of stone wall the slope of the equation increases as the roughness increases which means that the effect of roughness on (h) increases as the velocity of the air increases, and hence, for each surface texture there may be a specific linear equation that relates h with v.

Upon comparing the above coefficients it can also be noticed that the effect of increasing the wall roughness is more pronounced than the effect of increasing the wind speed. The average increasing in h is about 200%, and in U is about 60% when the wall roughness is changed from smooth to rough. This is larger than the average increase of 33% in h and 28% in U when the wind speed changes from low to high. This result put more emphasis on the wall texture from a heat transfer point of view.

Comparing the U values only, it can be seen also that the surface texture affects those values at wind speed of 0.5 m/s more than it dose at wind speed of 1.6 m/s.

6.4 Theoretical Fin Model Compared to Experimental Results

The modeling of the wall roughness as fins stems from the fact that the type of texture of the stone has a shape of an extended surface, and this extended irregular shape repeats itself through the single stone. In other words the type of irregularity can be defined, and each texture can be known just by looking at it, and this is why each type of texture has its own identity

(hammered “Musamsam”, Punched “Mufajjar” and Rough-Surface “Tubzeh”).

The concept of modeling here means finding accepted dimensions of different types of fins that give the same thermal performance of the different types of texture. The number of fins that is associated with each type of stone walls does not represent the degree of roughness, but it rather represents the number of domes of the texture, in other words, it represent the number of times the irregular shape repeats itself.

From tables 5.13 to 5.15, it is noticed that the fin length (L) has its greatest value for the rough-surface stone regardless of the fin model used. This is expected since the rough surface stone has the highest degree of roughness, and L is an indication of roughness. The second highest value of L is for the punched stone then for the hammered stone, which is reasonable again and agrees with the degree of roughness each stone represents.

The dimensions of fins that are tabulated in tables 5.13, 5.14 and 5.15 differ from type to type of stone texture. The largest dimension of fins is for rough - surface stone, and the lowest is for hammered stone, bearing in mind that the smooth stone has no fins to measure.

The model was used to calculate the heat transfer rate according to the dimensions of each type of fins. The results are tabulated in tables 3.16 to 3.18. From these tables, it is noticed that the heat - transfer rate is not far from the experimental value of 48 Watt. The values of heat transfer rate show that the pin fin model always gives values which are less than the experimental value of 48 Watt. This means that the dimensions of fins used in the model are rather small. The dimensions of the fins concluded from the models are based on two sources: i) The volume of the array of fins measured from the sand box technique, and ii) The estimation of the distance between the fin centers. The length of the fin depends only on the fin volume (V_f) and the distance between the fins. The cross - sectional area depends on the number of the fins in the array. Since the pin fin model gives values of heat transfer rate less than the experimental value, this means that the total effectiveness of the fin is small, i.e. the dimensions of the fin is small. Looking at the results shown in tables 3.16 to 3.18, one can notice that the length of the pin fin model is very large, furthermore, it is larger than the largest protrusion of the stone. For example, the largest length of the texture of the rough-surface is around 5 cm, and from table 3.18 it is almost 10.5 cm which is far away from the real stone dimensions compared with the rectangular and trapezoidal fin models. This can be explained in table 6.4

Table 6.4: Length of fins

wall type	L_r (mm)	L_p (mm)	L_t (mm)	roughness largest length (mm)
hammered	0.59	1.51	0.59	1.00
punched	5.03	12.82	5.031	10.00
rough	41.20	104.97	41.20	50.00

The reason why the length of the pin fin is large is that the type of the distribution of the pin fins differs from that of the longitudinal types. This makes the unfinned area of the stone wall to be large, and since the volume of the fins is the same for all fin types, the length of the pin fin must be large. Another reason that makes the unfinned area to be large is the distance between the fins (δ). In this work this distance is chosen to be $2D$ for pin fins. The dimensions of the trapezoidal and rectangular fin arrays are within the reasonable range, and heat transfer calculated theoretically by these models show that these models are closer to the experimental results than those of the pin fin.

The trapezoidal model of the rough surface wall shows that this model does not differ from the experimental value, which means that this model is a real representative of the rough - surface wall.

The model was used also to compute the convective and overall heat transfer coefficients of the different wall types as explained in the previous chapter. A comparison between the model and the experimental heat transfer coefficients are shown in tables 6.5 and 6.6 below. The subscript r, p and t under h and U in those tables refer to rectangular, pin and trapezoidal fin models:

Table 6.5: Convective heat coefficient (model versus experiment)

h (W/m ² °C)		hammered		punched		rough	
		v = 0.5 m/s	v = 1.6 m/s	v = 0.5 m/s	v = 1.6 m/s	v = 0.5 m/s	v = 1.6 m/s
M O D E L	h_r	7.8	10.71	11.29	14.23	12.834	16.87
	h_p	6.54	8.88	8.164	10.73	10.27	13.67
	h_t	8.11	11.16	10.65	13.53	11.999	15.83
	h_{exp}	6.87	9.60	9.60	12.00	12.00	16.00

Table 6.6: Overall heat-transfer coefficient (model versus experiment)

U (W/m ² °C)		hammered		punched		rough	
		v = 0.5 m/s	v = 1.6 m/s	v = 0.5 m/s	v = 1.6 m/s	v = 0.5 m/s	v = 1.6 m/s
M O D E L	U _r	4.2	5.95	6.27	7.115	6.417	7.19
	U _p	3.52	4.93	4.54	5.37	5.135	5.9
	U _t	4.37	6.2	5.90	6.77	6.00	6.78
	U _{exp}	3.69	5.33	5.33	6.00	6.00	6.87

The same arguments of the heat transfer rate can be made for the heat transfer coefficients, since the heat - transfer depends linearly on the value of the heat transfer rate. It can be noticed that the values of the heat transfer coefficients for pin fin model are always smaller than the experimental values. Also the values of the trapezoidal model for the rough surface stone walls are the same as the experimental values.

CHAPTER 7

CONCLUSIONS AND RECOMMENDATIONS

7.1 Conclusions

From the previous study, one can conclude the followings:

1. The overall heat transfer coefficient of the stone wall depends on the type of texture of the stone wall. The overall heat-transfer coefficient has its greatest value for rough-surface stone. The heat transfer coefficient is less for punched stone, then for hammered stone and it is lowest value is for smooth-surface stone . The value of U may increase from 43% to 75% for a rough (Tobzeh) stone over that of a smooth stone.
2. The same is applied for the convective heat-transfer coefficient (h) which depends on the type of texture of the stone wall. The value of h also increases as the roughness increases. The value of h may increase up to 200% for a rough (Tobzeh) stone over that of a smooth stone.

3. The surface texture of the stone wall acts on the wall like fins, and each type of texture has different fin dimension. The fin model of the stone walls gives reasonable fin dimensions for each type of texture. There is a considerable agreement between the fin model and the experimental results. The best model was that of a trapezoidal fin.

7.2 Recommendations

1. Effort should be made to modify the U - values of stone walls listed in the National Building code of Jordan to take into account the type of stone wall texture.
2. More researches and studies are recommended on various stone textures such as the “Barrel” type, which was not covered in this work. This type of texture may be compared specially with the “Tobzeh” type of stone to establish the effect of thickness versus that of surface area.
3. The future work should be reported with higher wind speeds up to 6 m/s to check if the texture effect becomes less significant at high wind speeds.
4. Other models may be tried for more agreement with the experimental work, such as hemispherical fins.
5. Other types of stone materials may be also tried, such as “Hayyan”, Ma’in”, ... etc. to study the effect of various stone texture on material from heat transfer point of view.

Following are recommendations to improve the apparatus:

1. It is highly recommended about the guard hot box apparatus used in this research to have for its cold room more sensitive thermostat that starts and stops within a temperature range not more than 1°C .
2. The thermocouples used in the apparatus should have larger accuracy (say 0.01°C) since each degree may make a jump in the calculation of heat-transfer coefficient.
3. The fan circuiting of the cold box should be fixed in order to rotate at higher speeds to give higher wind speeds as recommended previously in item 3.
4. A reliable wind anemometer should be installed inside the cold box with a connection to read out on the out side in order to be able to read the wind speed while the cold box is completely closed.

REFERENCES

- 1) Ray, B. B.: "Free and Forced Convection from Heated Cylinders in Air", Proc. Indian Ass. Cultiv., Vol. 6, 1920, PP. 95-107.
- 2) American Society of Heating, Refrigerating and Air-Conditioning Engineers, ASHRAE Handbook of Fundamentals, Atlanta, 1993, PP. 1-347.
- 3) National Building Code of Jordan, Vol. 13, 1st Ed., Amman, 1985, PP. 1-217.
- 4) Prasolov, R. S.: "The Effects of Surface Roughness of Horizontal Cylinders on Heat Transfer to Air", Inzhenerno Fizicheskji Zharnal, Vol. 4, 1961, PP. 3-7.
- 5) Jofre, R. J. and Barron, F.: "Free Convection Heat Transfer to a Rough Plate", ASME Paper, No.67-WA/HT, 1967, PP.1-3.
- 6) Eckert, E. R. G. and Jackson, T. W.: "Analysis of Turbulent Free Convection Boundary Layer on Flat Plate", NACA Report, No. 1015, 1951.

- 7) Fujii, T., Fujii, M. and Takeuchi, M.: "Influence of Various Surface Roughness on The Natural Convection ", International Journal of Heat and Mass Transfer, Vol. 16, 1973, PP. 629-640.
- 8) Sastry, C. V., Murthy, V. N. and Sarma, P. K.: "Effect of Discrete Wall Roughness on Free Convection Heat Transfer From a Vertical Tube", In Heat Transfer and Turbulent Buoyancy, Vol. 2, Hemisphere, Washington, D. C., 1976, PP. 651-661.
- 9) Anderson, R. and Bohn, M.: "Heat-Transfer Enhancement in Natural Convection Enclosure Flow ", Journal of Heat Transfer, Vol. 108, 1986, PP. 330-336.
- 10) Shakerin, S., Bohn, M. and Loehrke: "Natural convection in an Enclosure with Discrete Roughness Elements on a Vertical Heated Wall", International Journal of Heat and Mass Transfer, Vol. 31, No. 7, 1988, PP. 1423-1430.
- 11) Bhavnani, S. H. and Bergles, A. E.: "Effect of Surface Geometry and Orientation on Laminar Natural Convection Heat Transfer From a Vertical Flat Plate with Transverse Roughness Elements ", International Journal of Heat and Mass Transfer, Vol. 33, No. 5, 1990, PP. 965-981.

- 12) Bhavnani, S. H. and Bergles, A. E.: "An Experimental Study of Laminar Natural Convection Heat Transfer From Wavy Surfaces ", ASME Heat Transfer, Vol. 96, 1988, PP. 173-180.
- 13) Kishinami, K., Saito, H. and Tokura, I.: "Experimental Study on Natural Convection Heat Transfer from a Vertical Wave Surface Heated at Convex/Concave Elements", Nippon Kikai Gakkai Ronbunshu B Hen, Vol. 56, No. 57, 1987, PP. 36-38.
- 14) Hosni, M. H., Coleman, H. W. and Taylor, R. P.: "Measurements and Calculations of Rough-Wall Heat Transfer in The Turbulent Boundary Layer", International Journal of Heat and Mass Transfer, Vol. 34, No. 45, 1991, PP. 1067-1082.
- 15) Bauman, F., Gadgil, A., Kamerud, R., Altmayer, E. and Nanstell, M.: "Convective Heat Transfer in Buildings: Recent Research Results ", ASHRAE Transaction, Vol. 89, No. 1, 1983, PP. 215-233.
- 16) Karlekar, B. V. and Desmond, R. M.: Heat Transfer, 2nd Ed., West Publishing, Minnesota, 1982, PP. 1-564.
- 17) Chapman, A. J.: Heat Transfer, 4th Ed., Macmillan Publishing Co., New York, 1984, PP. 1-402.

- 18) ASTM Standards, “Standard Test Method for Steady-State Thermal Performance of Building Assemblies by Means of Guarded Hot Box”, ASTM Handbook, 1987, PP. C-236-87 .

APPENDIX A

DATA TABLES

A.1 Smooth-Surface Wall:

Table A.1: Smooth wall with high speed: metering box

Test	T_h (°C)								
	1	2	3	4	5	6	7	8	9
1	16	16	16	15	16	16	16	16	16
2	18	18	18	18	18	17	18	18	18
3	20	20	20	20	21	20	21	20	20
4	22	22	22	22	22	22	22	22	22
5	24	24	24	24	24	24	24	24	24
6	26	26	26	26	27	26	26	27	26
7	28	28	28	28	28	28	28	29	28

Table A.2: Smooth wall with high speed: guard box

Test	T _g (°C)		
	1	2	3
1	16	16	16
2	18	18	18
3	20	20	20
4	22	22	22
5	24	24	24
6	26	26	26
7	28	28	28

Table A.3: Smooth wall with high speed: cold box

Test	T _c (°C)								
	1	2	3	4	5	6	7	8	9
1	6	6	5	6	6	6	6	6	6
2	8	8	7	8	8	8	8	8	8
3	10	10	9	10	10	10	10	10	10
4	12	12	11	12	12	12	12	12	12
5	14	14	13	14	14	14	14	14	14
6	16	16	15	16	16	16	16	16	16
7	18	18	17	18	18	18	18	18	18

Table A.4: Smooth wall with high speed: wall hot surface

Test	T_1 (°C)				
	1	2	3	4	5
1	13	13	13	13	13
2	15	15	15	15	16
3	16	17	17	17	17
4	19	19	20	19	19
5	21	21	21	21	21
6	23	23	24	23	23
7	25	25	25	25	25

Table A.5: Smooth wall with high speed: wall cold surface

Test	T_2 (°C)				
	1	2	3	4	5
1	12	12	12	12	12
2	14	14	14	14	15
3	16	16	17	16	16
4	18	18	18	18	18
5	20	20	20	20	21
6	22	22	22	21	22
7	24	24	24	24	24

Table A.6: Smooth wall with low speed: metering box

Test	T_h (°C)								
	1	2	3	4	5	6	7	8	9
1	16	16	16	16	16	16	16	16	16
2	18	18	18	15	18	18	19	18	19
3	20	20	20	16	20	20	21	20	20
4	22	22	22	18	22	22	23	22	22
5	24	24	24	20	24	24	25	24	24
6	26	26	26	21	26	26	27	26	26
7	28	28	28	25	28	28	28	28	28

Table A.7: Smooth wall with low speed: guard box

Test	T_g (°C)		
	1	2	3
1	16	16	16
2	18	18	18
3	20	20	20
4	22	22	22
5	24	24	24
6	26	26	26
7	28	28	28

Table A.8: Smooth wall with low speed: cold box:

Test	T_c (°C)								
	1	2	3	4	5	6	7	8	9
1	2	0	2	2	2	2	1	2	2
2	4	4	4	4	3	4	3	4	4
3	6	6	6	6	6	6	6	6	6
4	8	8	8	8	8	8	8	8	8
5	10	10	10	10	9	10	10	10	10
6	12	12	12	12	12	12	12	12	11
7	14	14	14	14	14	14	14	14	14

Table A.9: Smooth wall with low speed: wall hot surface

Test	T_1 (°C)				
	1	2	3	4	5
1	11	11	11	11	11
2	13	13	13	13	13
3	15	15	15	15	15
4	17	17	17	17	17
5	19	19	19	19	19
6	21	21	21	21	21
7	23	23	23	23	23

Table A.10: Smooth wall with low speed: wall cold surface

Test	T_2 (°C)				
	1	2	3	4	5
1	10	10	10	10	10
2	12	12	12	12	12
3	14	14	14	14	14
4	16	16	16	16	16
5	18	18	18	18	18
6	20	20	20	20	20
7	22	22	22	22	22

A.2 Hammered-Surface Wall:

Table A.11: Hammered wall with high speed: metering box

Test	T_h (°C)								
	1	2	3	4	5	6	7	8	9
1	16	15	16	15	16	16	16	16	16
2	18	18	18	18	18	18	18	18	18
3	20	19	20	19	20	20	20	20	20
4	22	22	22	21	22	22	22	22	21
5	24	23	23	24	24	24	24	24	23
6	26	26	26	26	26	25	26	26	25
7	27	27	28	28	28	28	28	28	28

Table A.12: Hammered wall with high speed: guard box

Test	T _g (°C)		
	1	2	3
1	16	16	16
2	18	18	18
3	20	20	20
4	22	22	22
5	24	24	24
6	26	26	26
7	28	28	28

Table A.13: Hammered wall with high speed: cold box

Test	T _c (°C)								
	1	2	3	4	5	6	7	8	9
1	7	7	7	7	7	9	7	7	7
2	9	9	9	9	9	10	9	9	9
3	11	11	11	11	11	12	11	11	11
4	13	12	13	12	12	13	12	12	12
5	15	15	16	15	15	16	15	15	15
6	17	17	18	17	17	18	17	17	17
7	19	19	19	19	19	20	19	19	19

Table 314: Hammered wall with high speed: wall hot surface

Test	T_1 (°C)				
	1	2	3	4	5
1	13	13	13	13	13
2	15	15	14	15	15
3	17	17	17	17	17
4	19	19	19	19	19
5	21	21	20	21	21
6	23	23	22	23	23
7	25	25	25	25	25

Table A.15: Hammered wall with high speed: wall cold surface

Test	T_2 (°C)				
	1	2	3	4	5
1	12	12	12	12	12
2	14	14	14	14	14
3	16	15	16	16	16
4	17	18	18	17	18
5	20	20	20	20	20
6	22	23	22	22	22
7	24	24	24	24	24

Table A.16: Hammered wall with low speed: metering box

Test	T_h (°C)								
	1	2	3	4	5	6	7	8	9
1	16	16	16	16	16	16	16	16	16
2	18	18	18	18	19	18	18	18	19
3	20	20	20	20	21	20	20	20	20
4	22	22	22	22	23	21	21	21	21
5	24	24	24	24	24	24	24	24	24
6	26	26	25	26	25	26	26	26	26
7	28	28	27	28	27	28	28	28	28

Table A.17: Hammered wall with low speed: guard box

Test	T_g (°C)		
	1	2	3
1	16	16	16
2	18	18	18
3	20	20	20
4	22	22	22
5	24	24	24
6	26	26	26
7	28	28	28

Table A.18: Hammered wall with low speed: cold box

Test	T_c (°C)								
	1	2	3	4	5	6	7	8	9
1	3	3	3	3	3	3	3	3	3
2	5	5	5	5	5	5	5	5	5
3	7	7	7	7	7	7	7	7	7
4	9	9	9	9	9	9	9	9	9
5	11	11	11	11	11	11	11	11	11
6	13	13	13	13	13	13	13	13	13
7	15	15	15	15	15	15	15	15	15

Table A.19: Hammered wall with low speed: wall hot surface

Test	T_1 (°C)				
	1	2	3	4	5
1	11	11	11	11	11
2	13	13	14	13	13
3	15	15	16	15	15
4	17	17	18	17	17
5	19	19	20	19	19
6	21	21	22	21	21
7	23	23	24	23	23

Table A.20: Hammered wall with low speed: wall cold surface

Test	T_2 (°C)				
	1	2	3	4	5
1	10	10	10	10	10
2	12	12	12	12	13
3	14	14	14	14	14
4	16	16	16	16	16
5	18	18	18	18	18
6	20	20	20	20	20
7	22	22	22	22	22

A.3 Punched-Surface Wall:

Table A.21: Punched wall with high speed: metering box

Test	T_b (°C)								
	1	2	3	4	5	6	7	8	9
1	16	16	16	16	15	16	15	16	16
2	18	18	18	18	18	18	19	18	18
3	20	20	20	20	20	20	23	20	20
4	22	22	22	22	22	22	25	22	22
5	24	24	24	24	24	24	26	24	24
6	26	26	25	26	25	26	28	26	26
7	28	28	28	28	28	28	27	28	28

Table A.22: Punched wall with high speed: guard box

Test	T _g (°C)		
	1	2	3
1	16	16	16
2	18	18	18
3	20	20	20
4	22	22	22
5	24	24	24
6	26	26	26
7	28	28	28

Table A.23: Punched wall with high speed: cold box

Test	T _c (°C)								
	1	2	3	4	5	6	7	8	9
1	8	8	8	8	8	8	8	8	8
2	10	10	10	10	10	10	10	10	10
3	12	12	12	12	11	12	11	12	11
4	14	14	14	14	14	13	14	13	14
5	16	16	16	16	15	16	15	16	16
6	18	18	18	17	18	18	17	18	18
7	20	20	20	20	20	20	21	20	21

Table A.24: Punched wall with high speed: wall hot surface

Test	T_1 (°C)				
	1	2	3	4	5
1	13	13	13	13	13
2	15	15	14	15	15
3	16	17	16	17	17
4	19	19	18	19	19
5	21	21	21	21	21
6	23	23	22	23	23
7	25	25	24	25	25

Table A.25: Punched wall with high speed: wall cold surface

Test	T_2 (°C)				
	1	2	3	4	5
1	12	12	12	12	11
2	13	14	14	14	15
3	16	16	16	16	17
4	17	18	18	18	19
5	19	20	20	20	21
6	22	22	22	22	23
7	23	24	24	24	25

Table A.26: Punched wall with low speed: metering box

Test	T_h (°C)								
	1	2	3	4	5	6	7	8	9
1	16	16	16	15	16	17	16	16	17
2	18	18	17	18	19	18	18	17	18
3	20	20	21	20	20	19	20	20	20
4	22	22	21	22	22	22	21	23	21
5	24	24	26	24	24	24	23	24	24
6	26	26	26	25	26	26	25	26	26
7	28	28	28	26	28	28	28	28	29

Table A.27: Punched wall with low speed: guard box

Test	T_g (°C)		
	1	2	3
1	16	16	16
2	18	18	18
3	20	20	20
4	22	22	22
5	24	24	24
6	26	26	26
7	28	28	28

Table A.28: Punched wall with low speed: cold box

Test	T_c (°C)								
	1	2	3	4	5	6	7	8	9
1	7	7	8	7	6	7	7	7	7
2	9	9	9	9	8	9	9	9	9
3	11	10	11	10	11	11	11	11	11
4	13	13	13	13	12	13	13	13	13
5	15	15	14	14	15	15	15	15	15
6	17	17	17	17	17	17	16	17	17
7	19	19	19	19	19	19	20	19	19

Table A.29: Punched wall with low speed: wall hot surface

Test	T_1 (°C)				
	1	2	3	4	5
1	13	13	13	13	13
2	15	15	15	15	15
3	17	17	17	17	17
4	19	19	19	19	19
5	21	21	21	21	21
6	23	23	23	23	23
7	25	25	25	25	25

Table A.30: Punched wall with low speed: wall cold surface

Test	T_2 (°C)				
	1	2	3	4	5
1	12	12	11	12	12
2	13	14	14	14	14
3	16	16	17	16	16
4	18	18	18	18	18
5	20	20	20	20	20
6	22	22	22	23	22
7	24	24	24	24	24

A.4 Rough -Surface Wall:

Table A.31: Rough wall with high speed: metering box

Test	T_h (°C)								
	1	2	3	4	5	6	7	8	9
1	16	16	15	16	17	16	17	16	16
2	18	18	18	17	18	18	18	19	18
3	20	20	21	20	20	21	21	20	20
4	22	22	22	22	22	23	23	22	22
5	24	24	25	24	24	25	24	25	24
6	26	25	25	26	26	26	26	26	26
7	28	28	28	28	27	28	27	28	28

Table A.32: Rough wall with high speed: guard box

Test	T _g (°C)		
	1	2	3
1	16	16	16
2	18	18	18
3	20	20	20
4	22	22	22
5	24	24	24
6	26	26	26
7	28	28	28

Table A.33: Rough wall with high speed: cold box

Test	T _c (°C)								
	1	2	3	4	5	6	7	8	9
1	9	9	10	9	9	10	9	9	9
2	11	11	11	11	11	11	11	12	12
3	13	13	13	15	13	14	13	13	13
4	15	15	15	15	15	15	15	14	14
5	17	17	17	17	17	17	17	17	17
6	19	18	19	18	19	18	18	18	19
7	21	20	20	21	21	21	20	21	21

Table A.34: Rough wall with high speed: wall hot surface

Test	T_1 (°C)				
	1	2	3	4	5
1	13	12	13	13	13
2	15	14	15	15	15
3	17	16	17	17	17
4	19	19	19	19	19
5	21	20	21	21	21
6	23	22	23	23	23
7	25	25	25	25	25

Table A.35: Rough wall with high speed: wall cold surface

Test	T_2 (°C)				
	1	2	3	4	5
1	12	12	12	11	11
2	14	14	14	14	13
3	16	16	16	15	16
4	18	18	18	18	18
5	20	20	20	19	19
6	22	22	22	21	21
7	24	24	24	23	24

Table A.36: Rough wall with low speed: metering box

Test	T_h (°C)								
	1	2	3	4	5	6	7	8	9
1	16	15	14	16	16	16	16	16	17
2	18	18	19	19	18	18	18	18	19
3	20	20	21	23	20	20	20	21	20
4	22	22	22	22	21	21	21	22	22
5	24	24	24	24	24	22	24	23	22
6	26	26	26	26	25	24	26	24	26
7	28	28	28	27	27	26	28	28	28

Table A.37: Rough wall with low speed: guard box

Test	T_g (°C)		
	1	2	3
1	16	16	16
2	18	18	18
3	20	20	20
4	22	22	22
5	24	24	24
6	26	26	26
7	28	28	28

Table A.38: Rough wall with low speed: cold box

Test	T_b (°C)								
	1	2	3	4	5	6	7	8	9
1	8	8	8	8	8	8	8	8	8
2	10	10	10	10	10	10	10	10	10
3	12	12	12	12	12	13	12	11	12
4	14	14	15	15	15	14	14	14	14
5	16	16	16	16	16	16	16	16	16
6	18	18	17	17	18	18	18	17	18
7	20	20	21	21	21	20	20	20	20

Table A.39: Rough wall with low speed: wall hot surface

Test	T_1 (°C)				
	1	2	3	4	5
1	13	13	13	13	13
2	15	15	15	15	15
3	17	17	17	17	17
4	19	19	19	19	20
5	21	21	21	21	21
6	23	23	23	23	22
7	25	25	25	25	25

Table A.40: Rough wall with low speed: wall cold surface

Test	T_2 (°C)				
	1	2	3	4	5
1	12	12	12	12	11
2	14	14	14	14	13
3	16	16	16	16	15
4	18	18	18	18	17
5	20	20	20	20	19
6	22	22	22	22	21
7	24	24	24	24	23

APPENDIX B

SAMPLE CALCULATION

To explain how the experimental results presented in tables 5.1 to 5.8 are obtained a sample calculation is presented here. The temperature values used in the calculations are the average values of the temperature data of Appendix A. All the equations used in the calculation are presented in chapter 3. For example, one may take any case from the previous tables (randomly) like data test number 2 of the hammered wall (table 5.3). Data taken during the test is as follows:

$$Q = 48 \text{ Watt}$$

$$A = 1.0 \text{ m}^2$$

$$T_h = 18 \text{ }^\circ\text{C}$$

$$T_1 = 15 \text{ }^\circ\text{C}$$

$$T_c = 9 \text{ }^\circ\text{C}$$

$$T_g = 18 \text{ }^\circ\text{C}$$

$$l = .05 \text{ m}$$

using the above data one can make the following calculation:

Thermal conductivity(k):

Using equation (3.2)

$$k = \frac{48 \times 0.05}{1 \times (15 - 14)} = 2.4 \text{ W / m}^\circ \text{ C}$$

Convective heat - transfer coefficient (h):

Using equation (3.3)

$$h = \frac{48}{1 \times (14 - 9)} = 9.6 \text{ W / m}^2 \cdot ^\circ \text{ C}$$

overall heat - transfer coefficient:

using equation (3.1)

$$U = \frac{48}{1 \times (18 - 9)} = 5.33 \text{ W / m}^2 \cdot ^\circ \text{ C}$$

theoretical heat - transfer coefficient:

using equation

$$h_{th} = 5.62 + (3.9 \times 1.6) = 11.86 \text{ W / m}^2 \cdot ^\circ \text{ C}$$

All the results that are tabulated are obtained in the same manner

الملخص

انتقال الحرارة في الجدران الخارجية الحجرية: تأثير نقش الحجر

إعداد

يوسف "محمد سعيد" محمد إبراهيم

إشراف

د. علي بدران

يتناول هذا البحث دراسة تأثير نقش سطح الحجر على انتقال الحرارة وخصوصاً على المعامل الكلي لانتقال الحرارة. لقد تمت الدراسة بشكل تجريبي وبشكل نظري أيضاً. وقد تم القيام بالجزء التجريبي باستخدام الطريقة القياسية المعتمدة لدى الجمعية الأمريكية للفحص والمواد (ASTM) والتي يرمز لها بـ C-236. تم استخدام جهاز الصندوق الحافظ للحرارة لفحص أربعة أنواع مختلفة من الجدران الحجرية المتوفرة في الأردن حرارياً. إن أنواع الجدران الحجرية المستخدمة في هذا البحث هي الحجر المنشور، الحجر المسمى محلياً (المسمسم)، المفجر و الطبزة.

لقد وجد تجريبياً أنه، وبالنسبة للأنواع الأربعة من الجدران التي تمت تجربتها تحت

نفس المقدار من كمية الحرارة أن المعامل الكلي لانتقال الحرارة (U) للجدار الحجري

455763

المتكون من الحجر الطبزة له أعلى قيمة ثم يليه النوع المفجر ثم المسمم ثم أخيراً

المنشور .

كما تمت دراسة نظرية لإيجاد نموذج رياضي لانتقال الحرارة خلال هذه الأنواع

من الجدران الحجرية. وكان النموذج الذي تم بحثه هو لجدار مستوٍ مع زعانف، وذلك

يمثل خشونة نقش سطح الحجر. وقد وضعت نماذج لهذه الزعانف وكانت من النوع

المستطيل والدائري و شبه المنحرف وقد أعطت هذه النماذج نتائج قريبة من النتائج

التجريبية . وخصوصاً نموذج شبه المنحرف والذي أعطى تشبيهاً جيداً للحجر الطبزة.